

UV/IR mixing in Non-Fermi Liquids

Ipsita Mandal¹ and Sung-Sik Lee^{1,2}

¹Perimeter Institute for Theoretical Physics, 31 Caroline St. N., Waterloo ON N2L 2Y5, Canada

²Department of Physics & Astronomy, McMaster University, 1280 Main St. W., Hamilton ON L8S 4M1, Canada
(Dated: September 28, 2022)

We study low-energy effective field theories for non-Fermi liquids with Fermi surfaces of general dimensions and co-dimensions. When the dimension of Fermi surface is greater than one, low-energy particle-hole excitations remain strongly coupled with each other across the entire Fermi surface. In this case, even the observables that are local in the momentum space (such as the Green's functions) become dependent on the size of the Fermi surface in singular ways, resulting in a UV/IR mixing. By tuning the dimension and co-dimension of the Fermi surface independently, we find perturbative non-Fermi liquid fixed points controlled by both UV/IR mixing and interactions.

I. INTRODUCTION

There have been intensive efforts to understand unconventional metallic states that lie outside the framework of Landau Fermi liquid theory^{1–19}. Among the goals are to construct minimal field theories that capture universal low-energy physics, understand the dynamics in controlled ways, and eventually come up with a systematic classification for non-Fermi liquids.

Non-Fermi liquids can arise when a gapless boson is coupled with a Fermi surface. One of the important criteria that determines the universal properties of non-Fermi liquids is the momentum carried by the critical boson. If the critical boson carries zero momentum, fermions lose coherence across the entire Fermi surface. The examples include the Ising-nematic critical point^{11,13,20–34} and the Fermi surface coupled with an emergent gauge field^{35–38}. When the critical boson carries a finite momentum at the spin density wave (SDW) or charge density wave (CDW) critical points^{12,14,15,19}, the electrons on hot spots (or hot lines) play a special role because they remain strongly coupled with the critical boson in the low-energy limit. Another important criterion that characterizes different types of non-Fermi liquids is the geometry of Fermi surface. Although non-Fermi liquids do not have a finite jump in the electron occupation number, Fermi surface can be still well-defined through weaker non-analyticities (such as power-law singularities) of the electron spectral function³⁹. The Fermi surface, identified from a non-analyticity of the spectral function in a non-Fermi liquid state, is inherited from that of the underlying Fermi liquid before the coupling with a gapless boson is turned on. The kinematic constraints imposed by the parent Fermi surface geometry are important in determining the nature of the resulting non-Fermi liquid. In this paper, our goal is to understand how the nature of non-Fermi liquids depends on the Fermi surface geometry for those cases where the critical boson carries zero momentum.

When the shape of the Fermi surface is globally convex in momentum space, there is no special point on the Fermi surface¹⁰. Then Fermi surface geometry is classified in terms of the dimension and co-dimension of Fermi surface. Throughout the paper, we will use m for the

dimension of Fermi surface and d for the space dimension. The co-dimension of Fermi surface is then $d - m$. d controls the strength of quantum fluctuations, and m controls the extensiveness of gapless modes. Although d and m are discrete in reality, we will treat them as continuously tunable parameters to find controlled examples from which physical dimensions can be approached. Regarding d , theories below upper critical dimensions flow to interacting non-Fermi liquids at low energies, whereas systems above upper critical dimensions are expected to be described by Fermi liquids. Concerning non-Fermi liquids below upper critical dimensions, theories with $m = 1$ are fundamentally different from those with $m > 1$. This is due to an emergent locality in momentum space that is present for $m = 1$, but not for $m > 1$ ⁴⁰. The locality has to do with the fact that observables that are local in momentum space, such as Green's functions, can be extracted from local patches in momentum space without having to refer to global properties of Fermi surface⁴¹. By exploiting the locality in momentum space, controlled non-Fermi liquid fixed points are found in patch descriptions for $m = 1$ ^{8,10,16,18,19}.

In contrast to the case with $m = 1$, non-Fermi liquids with $m > 1$ are less well-understood. The naive scaling based on the patch description breaks down as the size of Fermi surface (k_F) qualitatively modifies the scaling through the Landau damping. This is due to a UV/IR mixing, where low-energy physics is affected by gapless modes on the entire Fermi surface in a way that their effects cannot be incorporated within the patch description through renormalization of local properties of the Fermi surface. In this sense, k_F becomes a ‘naked scale’ for $m > 1$.

Let us elaborate on the origin of the UV/IR mixing. In a renormalizable relativistic quantum field theory, the UV cut-off enters the low-energy effective theory only through the renormalized parameters that can be defined at a momentum scale far below the UV cut-off. For example, in QED, one can extract any observable at a momentum $k_1 \ll \Lambda$ solely in terms of the renormalized mass and charge measured at another momentum $k_2 \ll \Lambda$ to the leading order in k_1/Λ , where Λ is a large momentum cut-off. This insensitivity of the long-distance physics to

the short-distance physics does not necessarily hold in the presence of Fermi surface. When $m > 1$, low-energy observables defined at a momentum near Fermi surface (such as Green's functions) cannot be described solely in terms of the effective couplings defined near that momentum.

When a critical boson, that is coupled to Fermi surface, has a large number of flavors or velocity much higher than the Fermi velocity, one can find a wide range of energy scale over which the effect of k_F can be ignored⁴². However, the UV/IR mixing becomes eventually important in the low-energy limit as long as the number of flavors and the velocity ratio are finite either through the Landau damping or through a superconducting instability⁴³. In this paper, we provide a controlled analysis that shows how interactions and the UV/IR mixing interplay to determine low-energy scalings in non-Fermi liquids with general $m > 1$.

The paper is organized as follows: In Sec. II, we introduce a theory which describes the Ising-nematic quantum critical point for a system with an m -dimensional Fermi surface embedded in d spatial dimensions. For general m , we identify the upper critical dimension $d_c(m)$ at which one-loop quantum corrections exhibit logarithmic divergences. Using $\epsilon = d_c(m) - d$ as an expansion parameter, one can perturbatively access the non-Fermi liquid states that arise in $d < d_c(m)$. Sec. III is devoted to the description of the dimensional regularization scheme and the beta function that describes the flow to the non-Fermi liquid fixed point. In Sec. IV, the RG equations for the renormalized Green's functions are derived. Based on the one-loop results, the dynamical critical exponent, anomalous dimensions and two-point functions are also computed. Sec. V discusses the physical manifestations of UV/IR mixing in physical dimensions. In Sec. VI, we demonstrate that the expansion is controlled in the small ϵ limit with fixed N , where N is the number of fermion flavors. In particular, we show that the one-loop critical exponents are not modified by the two-loop (and possibly by all higher-loop) corrections for $m > 1$ due to the UV/IR mixing. We finish with a summary and some outlook in Sec. VII. Details on the computation of the Feynman diagrams upto two-loop order can be found in the appendix.

II. MODEL

We first consider an m -dimensional Fermi surface, which is coupled with a critical boson whose momentum is centered at $Q = 0$ in $d = (m + 1)$ space dimensions. One way of characterizing non-Fermi liquids is through scaling behaviors of the fermion and boson Green's functions. For this purpose, it is convenient to focus on the point (say K^*) at which the fermion Green's function is defined. At low energies, fermions are mainly scattered along the tangential directions by the critical boson. In the presence of the inversion symmetry, fermions

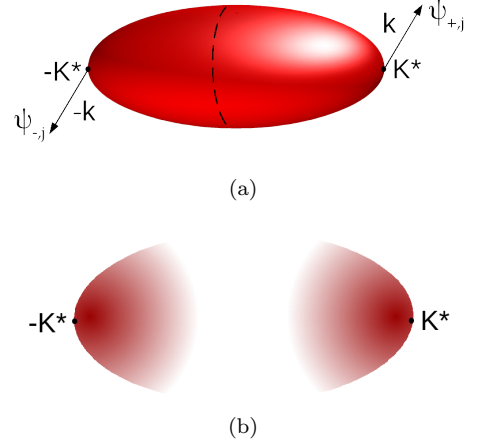


FIG. 1. (a) A compact Fermi surface can be divided into two halves centered at $\pm K^*$. For each half, a separate fermionic field is introduced. (b) The compact Fermi surface is approximated by two sheets of non-compact Fermi surfaces with a momentum regularization that suppresses modes far away from $\pm K^*$.

near K^* are most strongly coupled with fermions near its anti-podal point $-K^*$, whose tangent space coincides with that of K^* . With this in mind, we divide the closed Fermi surface into two halves centred at momenta K^* and $-K^*$ respectively, and introduce separate fermionic fields $\psi_{+,j}$ and $\psi_{-,j}$ representing the corresponding halves, as shown in Fig. 3. In this coordinate system, the action is written as

$$\begin{aligned}
 S = & \sum_{s=\pm,j} \int dk \psi_{s,j}^\dagger(k) \left[ik_0 + sk_1 + \mathbf{L}_{(k)}^2 + H(\mathbf{L}_{(k)}^2) \right] \psi_{s,j}(k) \\
 & + \frac{1}{2} \int dk \left[k_0^2 + k_1^2 + \mathbf{L}_{(k)}^2 \right] \phi(-k) \phi(k) \\
 & + \frac{1}{\sqrt{N}} \sum_{s=\pm,j} \int dk dq e_s \phi(q) \psi_{s,j}^\dagger(k+q) \psi_{s,j}(k). \quad (1)
 \end{aligned}$$

Here k is the $(d+1)$ -dimensional energy-momentum vector with $dk \equiv \frac{d^{d+1}k}{(2\pi)^{d+1}}$. $\psi_{+,j}(k_0, k_i)$ ($\psi_{-,j}(k_0, k_i)$) represents the fermion field with flavor $j = 1, 2, \dots, N$, frequency k_0 and momentum $K_i^* + k_i$ ($-K_i^* + k_i$) with $1 \leq i \leq d$. k_1 and $\mathbf{L}_{(k)} \equiv (k_2, k_3, \dots, k_d)$ represent the momentum components perpendicular and parallel to the Fermi surface at $\pm K^*$, respectively. The momentum is rescaled such that the absolute value of the Fermi velocity, and the quadratic curvature of the Fermi surface at $\pm K^*$, are equal to one. Because the Fermi surface is locally parabolic, it is natural to set the scaling dimension of k_1 ($\mathbf{L}_{(k)}$) to be 1 (1/2). $H(\mathbf{L}_{(k)}^2) = \sum_{n=3}^{\infty} \sum_{i_1, \dots, i_n=2}^d \frac{c_{i_1, \dots, i_n}}{k_F^{\frac{n-2}{2}}} k_{i_1} \dots k_{i_n}$ denotes cubic and higher order terms in $\mathbf{L}_{(k)}$, where k_F is a scale of dimension 1. The range of $\mathbf{L}_{(k)}$ in $\int dk$ is set by the size of the Fermi surface, which is of order $k_F^{1/2}$ in this coordinate

system. The Yukawa coupling has been also expanded around $\pm K^*$, and only the momentum independent part is kept. For the Ising-nematic quantum critical point, which we consider in this paper, we have $e_+ = e_-$.

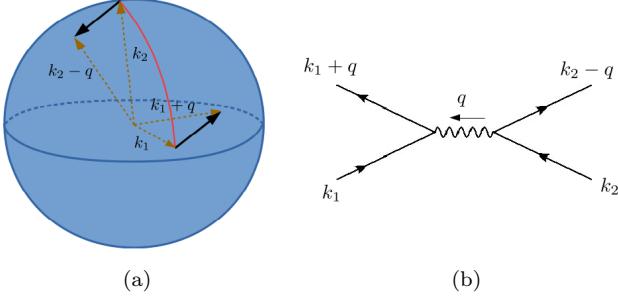


FIG. 2. For $m > 1$, any two points on the Fermi surface have at least $(m - 1)$ common tangent vectors.

The action is reminiscent of patch theories that have been used to describe non-Fermi liquids with one-dimensional Fermi surface. However, there is also an important difference between the theory with general $m > 1$ and the one with $m = 1$. For $m > 1$, any two points on the Fermi surface have at least $(m - 1)$ common tangent vectors, and the whole Fermi surface remains strongly coupled at low energies. Fig. 2 illustrates this point for a spherical Fermi surface embedded in a three-dimensional momentum space. Suppose that two fermions at general momenta k_1, k_2 are scattered to $k_1 + q, k_2 - q$ by exchanging a boson with small momentum q . Because q can be tangential to the Fermi surface both at k_1 and k_2 for $m > 1$, the fermions can stay near the Fermi surface before and after scattering. Therefore any two fermions on the Fermi surface remain strongly coupled in the low energy limit even though the processes with large momentum exchanges are suppressed. For $m = 1$, such low-energy scattering is not present except for the two anti-podal points. Because of the coupling that is global in the momentum space, the theory with $m > 1$ is ill-defined in the $k_F \rightarrow \infty$ limit unlike the case with $m = 1$. In other words, low-energy (IR) observables, such as the fermion and boson Green's functions near $k = 0$, can not be defined until global properties, such as the size and shape, of the Fermi surface are specified at large momenta (UV) for $m > 1$. In Fermi liquids, this UV/IR mixing is encoded in the Landau parameters which are non-local in the momentum space. It is our goal to understand consequences of the UV/IR mixing in non-Fermi liquid states with $m > 1$.

The scale k_F in $H(\mathbf{L}_{(k)}^2)$ provides a large momentum cut-off along the directions parallel to the Fermi surface. Although irrelevant by power counting, it is crucial to include the higher order terms to keep the information that the Fermi surface is compact. In principle, one has to keep an infinite set of independent parameters c_{i_1, \dots, i_n} that encodes the precise shape of the Fermi surface away

from K^* . Here we consider a simplified ‘UV regularization’ which keeps the essential physics of the higher-order terms, but is simple enough to be amenable to an analytic treatment. Specifically, we consider a regularized kinetic term

$$\sum_{s,j} \int dk \psi_{s,j}^\dagger(k) \left[ik_0 + sk_{d-m} + \mathbf{L}_{(k)}^2 \right] \psi_{s,j}(k) \exp \left\{ \frac{\mathbf{L}_{(k)}^2}{k_F} \right\}. \quad (2)$$

Here we keep the dispersion parabolic, but the exponential factor effectively makes the size of the Fermi surface finite by damping the propagation of fermions with $|\mathbf{L}_{(k)}| > k_F^{1/2}$, as is illustrated in Fig. 1(b).

In order to control the Yukawa coupling and the strength of UV/IR mixing independently, we tune both the dimension^{42–44} and the co-dimension of the Fermi surface^{18,19,45}. To keep the analyticity of the theory in momentum space (locality in real space) with general co-dimensions, we introduce a spinor^{18,19} $\Psi_j^T(k) = (\psi_{+,j}(k), \psi_{-,j}^\dagger(-k))$ to write an action that describes an m -dimensional Fermi surface embedded in the d -dimensional momentum space:

$$S = \sum_j \int dk \bar{\Psi}_j(k) \left[i\mathbf{\Gamma} \cdot \mathbf{K} + i\gamma_{d-m} \delta_k \right] \Psi_j(k) \exp \left\{ \frac{\mathbf{L}_{(k)}^2}{\mu k_F} \right\} + \frac{1}{2} \int dk \mathbf{L}_{(k)}^2 \phi(-k) \phi(k) + \frac{ie\mu^{x/2}}{\sqrt{N}} \sum_j \int dk dq \phi(q) \bar{\Psi}_j(k+q) \gamma_{d-m} \Psi_j(k). \quad (3)$$

Here, $\mathbf{K} \equiv (k_0, k_1, \dots, k_{d-m-1})$ includes the frequency and the first $(d-m-1)$ components of the d -dimensional momentum vector, $\mathbf{L}_{(k)} \equiv (k_{d-m+1}, \dots, k_d)$ and $\delta_k = k_{d-m} + \mathbf{L}_{(k)}^2$. In the d -dimensional momentum space, k_1, \dots, k_{d-m} ($\mathbf{L}_{(k)}$) represent(s) the $(d-m)$ (m) directions perpendicular (tangential) to the Fermi surface. $\mathbf{\Gamma} \equiv (\gamma_0, \gamma_1, \dots, \gamma_{d-m-1})$ represents the gamma matrices associated with \mathbf{K} . Since we are interested in co-dimension $1 \leq d-m \leq 2$, we consider only 2×2 gamma matrices with $\gamma_0 = \sigma_y$, $\gamma_{d-m} = \sigma_x$ and $\bar{\Psi} \equiv \Psi^\dagger \gamma_0$.

The leading terms in the quadratic action in Eq. (3) are invariant under the scale transformations:

$$\mathbf{K} = \frac{\mathbf{K}'}{b}, \quad k_{d-m} = \frac{k'_{d-m}}{b}, \quad \mathbf{L}_{(k)} = \frac{\mathbf{L}'_{(k)}}{\sqrt{b}}, \quad \Psi_j(k) = b^{\frac{2d+4-m}{4}} \Psi'_j(k'), \quad \phi(k) = b^{\frac{2d+4-m}{4}} \phi'(k'). \quad (4)$$

In the quadratic action of the boson, only $\mathbf{L}_{(k)}^2 \phi^*(k) \phi(k)$ is kept, because $|\mathbf{K}|^2 + k_{d-m}^2$ is irrelevant under the scaling where k_0, k_1, \dots, k_{d-m} have dimension 1 and k_{d-m+1}, \dots, k_d have dimension 1/2. In the presence of the $(m+1)$ -dimensional rotational symmetry, all components of k_{d-m}, \dots, k_d should be equivalent. The reason why k_{d-m} is treated differently from $\mathbf{L}_{(k)} = (k_{d-m+1}, \dots, k_d)$ is because bosons that are strongly coupled to the fermions

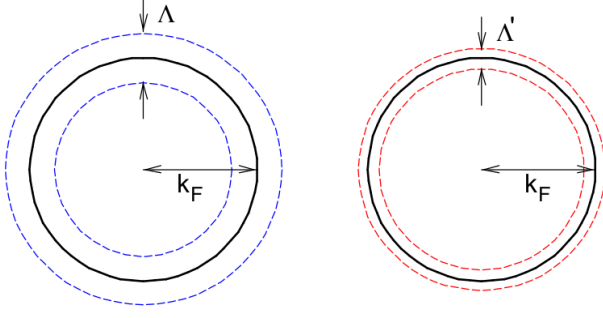


FIG. 3. As the high-energy modes away from the Fermi surface are integrated out, the ratio k_F/Λ grows. k_F is the size of the Fermi surface and Λ is the energy cut-off perpendicular to the Fermi surface. For $m > 1$, the Green's functions are singular in the $k_F/\Lambda \rightarrow \infty$ limit, which results in the UV/IR mixing.

around $\pm K^*$ have momentum $|\mathbf{L}_{(k)}| \gg k_{d-m}$. Therefore we ignore the dependence on k_{d-m} in the boson kinetic term in the effective theory that describes the regions around $\pm K^*$.

The scaling dimension of the Yukawa coupling is

$$x = \frac{4 + m - 2d}{2}. \quad (5)$$

Here, e is dimensionless and μ is a mass scale. We also define a dimensionless parameter for the Fermi momentum, $\tilde{k}_F = k_F/\mu$. The spinor has the energy dispersion with two bands, $E_k = \pm \sqrt{\sum_{i=1}^{(d-m-1)} k_i^2 + \delta_k^2}$, which gives an m -dimensional Fermi surface embedded in the d -dimensional momentum space, defined by the $d-m$ equations: $k_i = 0$ for $i = \{1, \dots, d-m-1\}$ and $k_{d-m} = -\mathbf{L}_{(k)}^2$.

Besides k_F and e , the theory implicitly has a UV cut-off for \mathbf{K} and k_{d-m} , which we denote as Λ . It is natural to choose $\Lambda = \mu$, and the theory has two important dimensionless parameters: e , $\tilde{k}_F = k_F/\Lambda$. If k is the typical energy at which we probe the system, the limit of interest is $k \ll \Lambda \ll k_F$. This is because Λ sets the largest energy (equivalently, momentum perpendicular to the Fermi surface) fermions can have, whereas k_F sets the size of the Fermi surface. We will consider the renormalization group flow generated by changing Λ and requiring that low-energy observables are independent of it. This is equivalent to a coarse-graining procedure of integrating out high-energy modes away from Fermi surface. Because the zero energy modes are not integrated out, k_F/Λ keeps increasing in the coarse graining procedure. We treat k_F as a dimensionful coupling constant that flows to infinity in the low-energy limit. Physically, this describes the fact that the size of the Fermi surface measured in the unit of the thickness of the thin shell around the Fermi surface diverges in the low-energy limit. This is illustrated in Fig. 3.

III. DIMENSIONAL REGULARIZATION

To access perturbative non-Fermi liquids, we fix m and tune d towards a critical dimension, at which quantum corrections depend logarithmically on Λ within the range $\Lambda \ll k_F$. The Yukawa coupling is dimensionless at

$$d'_c(m) = \frac{4 + m}{2}. \quad (6)$$

However, it turns out that this is not the actual upper critical dimension at which the quantum corrections diverge logarithmically in Λ . The shift of the upper critical dimension is a sign that k_F enters the low-energy physics in a way that is singular in the large k_F limit, resulting in UV/IR mixing.

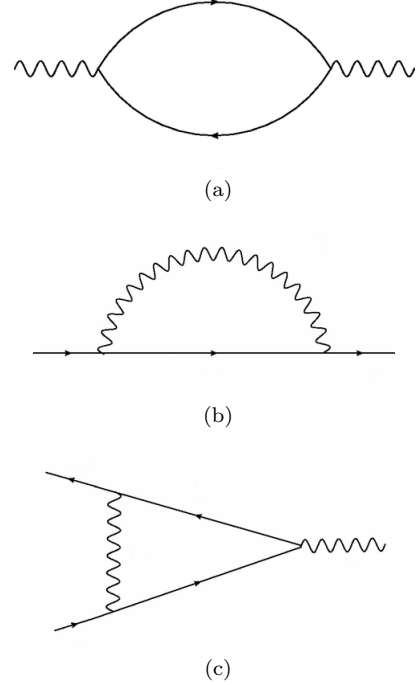


FIG. 4. The one-loop diagrams for the boson self-energy (a), the fermion self-energy (b), and the vertex correction (c). Solid lines represent the bare fermion propagator, whereas wiggly lines in (b) and (c) represent the dressed boson propagator which includes the one-loop self-energy in (a).

In order to identify the actual upper critical dimension, we consider the one-loop quantum corrections. Since the bare boson propagator is independent of k_0, \dots, k_{d-m} , the loop integrations involving it are ill-defined, unless one resums a series of diagrams that provides a non-trivial dispersion along those directions. This amounts to rearranging the perturbative expansion such that the one-loop boson self-energy is included at the 'zero'-th order. The dressed boson propagator, which includes the one-

loop self-energy (Fig. 4(a)), is given by

$$D_1(k) = \frac{1}{\mathbf{L}_{(k)}^2 + \beta_d e^2 \mu^x \frac{(\mu \tilde{k}_F)^{\frac{m-1}{2}} |\mathbf{K}|^{d-m}}{|\mathbf{L}_{(k)}|}}, \quad (7)$$

to the leading order in k/k_F , for $|\mathbf{K}|^2/|\mathbf{L}_{(k)}|^2$, $\delta_k^2/|\mathbf{L}_{(k)}|^2 \ll k_F$. Here $\beta_d = \frac{\Gamma^2(\frac{d-m+1}{2})}{\frac{2d+m-1}{2} \pi^{\frac{d-1}{2}} |\cos\{\frac{\pi(d-m+1)}{2}\}| \Gamma(\frac{d-m}{2}) \Gamma(d-m+1)}$ is a parameter of the theory that depends on the shape of the Fermi surface. See Appendix A for the derivation of the one-loop self-energies. Since the boson propagator depends on e , the higher-loop diagrams are no longer suppressed by e^2 , but by a fractional power of e^{18} . Moreover, the boson self-energy diverges in the $k_F \rightarrow \infty$ limit for $m > 1$. This is due to the fact that the Landau damping gets stronger for a system with a larger Fermi surface, as the boson can decay into particle-hole excitations that encompass the entire Fermi surface for $m > 1$. This is in contrast with the case for $m = 1$, where a low-energy boson with a given momentum can decay into particle-hole excitations only near the isolated patches whose tangent vectors are parallel to that momentum. For $m = 1$, k_F drops out in Eq. (7), which indicates the absence of UV/IR mixing. Eq. (7) is valid when there exists at least one direction that is tangential to the Fermi surface, and it should not be extended to the cases with $m < 1$ for which the conventional quantum field theories work well. From now on, we will focus on the case with $m > 1$.

The apparent lack of rotational symmetry in the space of k_{d-m}, \dots, k_d in Eq. (7) is because the expression is valid only for the boson whose momentum is almost tangential to the Fermi surface at points $\pm K^*$ as is discussed below Eq. (4). For the boson propagator with general momentum, $|\mathbf{L}_{(k)}|$ in Eq. (7) should be replaced by $\sqrt{k_{d-m}^2 + \dots + k_d^2}$ in the presence of $(m+1)$ -dimensional rotational symmetry. This is because for any given boson momentum k , one can always find a point on the Fermi surface where k is tangential to the Fermi surface. If one chooses a coordinate system where $k_{d-m} = 0$, the boson self-energy takes the exactly same form as in Eq. (7). Since we can do this for any k , the boson propagator with general momentum should be independent of the direction in the space of (k_{d-m}, \dots, k_d) . In the following, we will use the expression in Eq. (7) because we are only interested in describing the Fermi surface near $\pm K^*$. The bosons that are strongly coupled to that region have momentum $k_{d-m} \ll |\mathbf{L}_{(k)}|$, and $\sqrt{k_{d-m}^2 + \dots + k_d^2}$ is re-

duced to $|\mathbf{L}_{(k)}|$.

By using the dressed boson propagator, we have computed the one-loop fermion self-energy $\Sigma_1(q)$ (Fig. 4(b)) in Appendix A 2. This blows up logarithmically in Λ at a new critical dimension

$$d_c(m) = m + \frac{3}{m+1}, \quad (8)$$

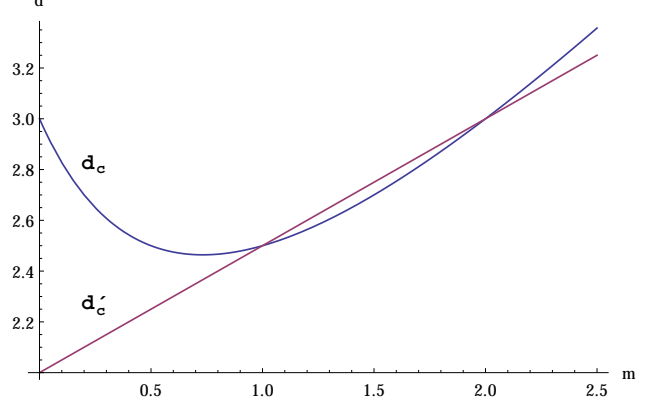


FIG. 5. The plots for d_c and d'_c as functions of m .

which is smaller than d'_c for general $1 < m < 2$. Fig. 5 shows the plots of d_c and d'_c as functions of m . Now we consider the space dimension $d = d_c(m) - \epsilon$. In the dimensional regularization scheme, the logarithmic divergence in Λ turns into a pole in $1/\epsilon$:

$$\Sigma_1(q) = \left(-\frac{e^{2(m+1)/3}}{\tilde{k}_F^{\frac{(m-1)(2-m)}{6}}} \frac{u_1}{N \epsilon} + \text{finite terms} \right) (i\mathbf{\Gamma} \cdot \mathbf{Q}), \quad (9)$$

to the leading order in q/k_F , where $u_1 = \frac{1}{\pi^{\frac{m-2}{2}} (4\pi)^{\frac{3}{2(m+1)}} 2^{m-1} |\sin\{(m+1)\pi/3\}| \beta_d^{\frac{2-m}{3}} (m+1)} \times \frac{\Gamma(\frac{m+4}{2(m+1)})}{\Gamma(m/2) \Gamma(\frac{2-m}{2(m+1)}) \Gamma(\frac{2m+5}{2(m+1)})}$. The one-loop vertex correction in Fig. 4(c) vanishes due to a Ward identity¹⁸.

It is noted that one can tune the dimension of Fermi surface from $m = 1$ to $m = 2$ while keeping ϵ small, thus providing a controlled description for any m between 1 and 2. This is possible because we are tuning m and d independently. For a given m , we tune d such that $\epsilon = d_c(m) - d$ is small. To remove the UV divergences in the $\epsilon \rightarrow 0$ limit, we add counterterms using the minimal subtraction scheme. Adding the counterterms to the original action, we obtain the renormalized action which gives the finite quantum effective action:

$$\begin{aligned}
S_{ren} = & \sum_j \int dk_B \bar{\Psi}_{Bj}(k_B) \left[i\mathbf{\Gamma} \cdot \mathbf{K}_B + i\gamma_{d-m}\delta_{k_B} \right] \Psi_{Bj}(k_B) \exp \left\{ \frac{\mathbf{L}_{(k),B}^2}{k_{F,B}} \right\} \\
& + \frac{1}{2} \int dk_B \mathbf{L}_{(k)}^2 \phi_B(-k_B) \phi_B(k_B) \\
& + \frac{ie_B}{\sqrt{N}} \sum_j \int dk_B dq_B \phi_B(q_B) \bar{\Psi}_{Bj}(k_B + q_B) \gamma_{d-m} \Psi_{Bj}(k_B), \tag{10}
\end{aligned}$$

where

$$\begin{aligned}
\mathbf{K} &= \frac{Z_2}{Z_1} \mathbf{K}_B, \quad k_{d-m} = k_{B,d-m}, \quad \mathbf{L}_{(k)} = \mathbf{L}_{(k),B}, \\
\Psi(k) &= Z_\Psi^{-1/2} \Psi_B(k_B), \quad \phi(k) = Z_\phi^{-1/2} \phi_B(k_B), \\
e_B &= Z_3^{-1/2} \left(\frac{Z_2}{Z_1} \right)^{(d-m)/2} \mu^{x/2} e, \quad k_F = \mu \tilde{k}_F, \tag{11}
\end{aligned}$$

with

$$Z_\Psi = Z_2 \left(\frac{Z_2}{Z_1} \right)^{(d-m)}, \quad Z_\phi = Z_3 \left(\frac{Z_2}{Z_1} \right)^{(d-m)}. \tag{12}$$

The subscript ‘‘B’’ denotes the bare quantities. To the one-loop order, we have $Z_n = 1 + \frac{Z_{n,1}}{\epsilon}$ with

$$\begin{aligned}
Z_{1,1} &= -\frac{e^{2(m+1)/3} u_1}{\tilde{k}_F^{\frac{(m-1)(2-m)}{6}} N}, \\
Z_{2,1} &= 0, \\
Z_{3,1} &= 0. \tag{13}
\end{aligned}$$

The one-loop beta functions, that dictate the flow of \tilde{k}_F and e with the increasing logarithmic length scale l , are given by

$$\frac{d\tilde{k}_F}{dl} = \tilde{k}_F, \tag{14}$$

$$\frac{de}{dl} = \left[\frac{\epsilon}{2} + \frac{(m-1)(2-m)}{4(m+1)} \right] e - \frac{u_1 \tilde{e}}{2N} e, \tag{15}$$

with

$$\tilde{e} \equiv \frac{e^{2(m+1)/3}}{\tilde{k}_F^{\frac{(m-1)(2-m)}{6}}}. \tag{16}$$

\tilde{k}_F increases under the RG flow because the size of the Fermi surface, measured in the unit of the floating energy scale $\mu \exp(-l)$, increases at low energies. The first term in the beta function of e indicates that e remains strictly relevant at $d = d_c(m)$ for $1 < m < 2$. However, the form

of the loop correction (the second term) implies that the higher order corrections are controlled not by e , but by an effective coupling \tilde{e} . This can be also checked for higher-order diagrams. The beta function for \tilde{e} , which no longer contains k_F , is given by

$$\frac{d\tilde{e}}{dl} = \frac{(m+1)\epsilon}{3} \tilde{e} - \frac{(m+1)u_1}{3N} \tilde{e}^2, \tag{17}$$

to order \tilde{e}^2 .

Eq. (17) shows that the effective coupling flows to an IR stable fixed point at

$$\tilde{e}^* = \frac{N\epsilon}{u_1} + \mathcal{O}(\epsilon^2). \tag{18}$$

For small ϵ , the interacting fixed point is perturbatively accessible despite the fact that the scaling dimension of the bare coupling e stays positive in the $\epsilon \rightarrow 0$ limit for $1 < m < 2$. Although e grows at low energies, the increase of the bare coupling is compensated by the Landau damping, which also increases with the effective size of the Fermi surface. The competition between the interaction and the Landau damping makes the effective coupling marginal at the new critical dimension d_c . It is interesting that k_F drops from the effective coupling not only for $m = 1$ but also for $m = 2$. For the latter case, the k_F dependence in the Landau damping cancels out the k_F dependence from the phase space of intermediate states in Fig. 4(b). However, the UV/IR mixing is present for all $m > 1$ because the Landau damping diverges in the large k_F limit.

IV. RENORMALIZATION GROUP EQUATIONS

The renormalized Green's functions, defined by $\left\langle \phi(k_1) \dots \phi(k_{n_\phi}) \Psi(k_{n_\phi+1}) \dots \Psi(k_{n_\phi+n_\psi}) \bar{\Psi}(k_{n_\phi+n_\psi+1}) \dots \bar{\Psi}(k_{n_\phi+2n_\psi}) \right\rangle = G^{(n_\psi, n_\psi, n_\phi)}(\{k_i\}; \tilde{e}, \tilde{k}_F, \mu) \delta^{d+1} \left(\sum_{i=1}^{n_\phi+n_\psi} k_i - \sum_{j=n_\phi+n_\psi+1}^{2n_\psi+n_\phi} k_j \right)$, satisfy the RG equations

$$\left\{ - \sum_{i=1}^{2n_\psi+n_\phi} \left(z \mathbf{K}_i \cdot \nabla_{K_i} + k_{i,d-m} \frac{\partial}{\partial k_{i,d-m}} + \frac{\mathbf{L}_{(k_i)}}{2} \cdot \nabla_{L_{(k_i)}} \right) - \frac{d\tilde{k}_F}{dl} \frac{\partial}{\partial \tilde{k}_F} - \frac{d\tilde{e}}{dl} \frac{\partial}{\partial \tilde{e}} + 2n_\psi \left(-\frac{2d_c - 2\epsilon + 4 - m}{4} + \eta_\psi \right) \right. \\ \left. + n_\phi \left(-\frac{2d_c - 2\epsilon + 4 - m}{4} + \eta_\phi \right) + d_c - \epsilon + 1 - \frac{m}{2} + (d_c - \epsilon - m)(z - 1) \right\} G^{(n_\psi, n_\psi, n_\phi)}(\{k_i\}; \tilde{e}, \tilde{k}_F, \mu) = 0. \quad (19)$$

Here the dynamical critical exponent z and the anomalous dimensions are given by

$$z^* = \frac{3}{3 - (m+1)\epsilon}, \quad \eta_\psi^* = \eta_\phi^* = -\frac{\epsilon}{2}, \quad (20)$$

to the one-loop order at the fixed point. It is remarkable that the exponents are insensitive to the details of the Fermi surface (such as β_d) despite the fact that patch scaling is violated by k_F . This vindicates our use of the exponential cut-off scheme in Eq. (2) which captures the compactness of the Fermi surface in a minimal way without including the details of the shape. The finite anomalous dimensions are the result of the dynamical balance between the two strongly relevant couplings, e and k_F . This is opposite to the case where finite anomalous dimensions result from a balance between two irrelevant ‘couplings’¹⁹.

From this, one can write down the general scaling form of the two-point functions at the IR fixed point as:

$$G^{(0,0,2)} = \frac{1}{(\mathbf{L}_{(k)}^2)^{2\Delta_\phi}} f_D \left(\frac{|\mathbf{K}|^{1/z^*}}{\mathbf{L}_{(k)}^2}, \frac{k_{d-m}}{k_F}, \frac{\mathbf{L}_{(k)}^2}{k_F} \right), \\ G^{(1,1,0)} = \frac{1}{|\delta_k|^{2\Delta_\psi}} f_G \left(\frac{|\mathbf{K}|^{1/z^*}}{\delta_k}, \frac{\delta_k}{k_F}, \frac{\mathbf{L}_{(k)}^2}{k_F} \right), \quad (21)$$

where $2\Delta_\phi = 1 - (z^* - 1) \left(\frac{3}{m+1} - \epsilon \right) - 2\eta_\phi^* = 1 + O(\epsilon^2)$, $2\Delta_\psi = 1 - (z^* - 1) \left(\frac{3}{m+1} - \epsilon \right) - 2\eta_\psi^* = 1 + O(\epsilon^2)$. To the one-loop order, the universal scaling functions are given by

$$f_D(X, Y, Z) = \left[1 + \beta_d \tilde{e}^{\frac{3}{m+1}} X^{\frac{3}{m+1}} Z^{-\frac{3(m-1)}{2(m+1)}} \right]^{-1}, \quad (22)$$

$$f_G(X, Y, Z) = -i \left[C (\mathbf{\Gamma} \cdot \hat{\mathbf{K}}) X + \gamma_{d-m} \right]^{-1}, \quad (23)$$

in the $Y, Z \rightarrow 0$ limit with fixed X . Here $C = \mu^{\frac{m+1}{3}\epsilon} \left\{ 1 - \frac{(m+1)\gamma\epsilon}{6} \right\}$, and γ is the Euler-Mascheroni constant. It is noted that f_D has a singular dependence on Z in the small Z limit. The absence of the sliding symmetry makes the fermion Green’s function depend on δ_k and $\mathbf{L}_{(k)}$ separately in general.

V. PHYSICAL RELEVANCE OF THE DIMENSIONAL EXPANSION

The motivation for the dimensional expansion is to understand the stark difference in the behaviors of

non-Fermi liquids in two and three dimensions. Non-Fermi liquids in two dimensions can at most have one-dimensional Fermi surface, for which k_F does not play an important role in the low-energy scaling. On the other hands, k_F enters as an important scale in three dimensions due to UV/IR mixing. Our goal is to understand how this transition occurs in a systematic way by tuning the dimension and co-dimension continuously. Although systems with non-integer dimensions are unphysical by themselves, they provide an insight on how dimension and co-dimension contribute to different behaviors of metals in the physical dimensions.

In physical dimension with $d = 3, m = 2$, k_F drops out in the effective coupling. However, the non-trivial UV/IR mixing still manifests itself in the dispersions of fermion and boson. Near $d = 3$, fermion has the dispersion $k_0 \sim k_x + L_k^2$, whereas the boson has the scaling $k_0 \sim L_k^3$ upto small corrections. Our theory provides a scaling consistent both for boson and fermion by including k_F as a dimensionful parameter of the theory. Boson and fermion can have different effective dynamical critical exponents at the scale-invariant fixed point, because the difference of the dynamical critical exponents is compensated by k_F . This is in contrast to the case with $m = 1$, where the dispersions of the boson and fermion obey the same scaling behavior. UV/IR mixing also plays an important role in suppressing higher-loop quantum corrections for $m > 1$. In the following section, we will examine the effect of k_F in higher-loop diagrams.

VI. EXPANSION PARAMETER

The present work is an extension of the early work¹⁸ which provides a controlled expansion for non-Fermi liquids supporting one-dimensional Fermi surface ($m = 1$). For $m = 1$, it was explicitly shown that two and three-loop diagrams are suppressed by positive powers of \tilde{e} , which is of the order ϵ . There also exists a general argument outlining why higher-loop diagrams are systematically suppressed by higher powers of \tilde{e} . The expansion here is different from an expansion in powers of $1/N$, and it does not suffer from the proliferation of planar diagrams in the $1/N$ expansion^{9,12}. Due to the addition of the extra co-dimensions, the density of states is suppressed at low energies. The weaker IR singularity allows one to have a controlled expansion for a sufficiently small ϵ . In the present paper, we have generalized this to the cases where the dimension of Fermi surface is greater than one ($m > 1$). For $m > 1$, the suppression of higher-

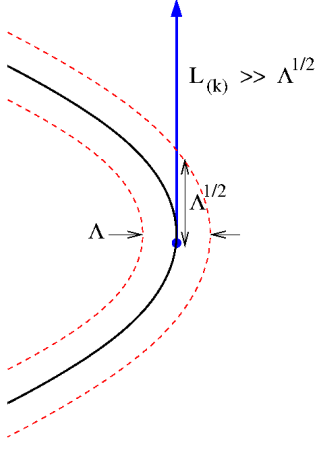


FIG. 6. A two-dimensional slice of an m -dimensional Fermi surface. The typical momentum carried by a boson is proportional to $\tilde{\alpha}^{1/3} \Lambda^{\frac{d-m}{3}} \sim \tilde{e}^{\frac{1}{m+1}} \left(\frac{k_F}{\Lambda} \right)^{\frac{m-1}{2(m+1)}} \Lambda^{1/2}$. For $m > 1$, this momentum is much larger than $\Lambda^{1/2}$ in the low-energy limit. As a result, the momentum transferred from a boson takes a fermion near the Fermi surface outside the thin shell of the UV cut-off. This leads to a suppression of the virtual particle-hole excitations by powers of Λ/k_F for $m > 1$.

loop diagrams by positive powers of \tilde{e} is unchanged. The difference for $m > 1$ is the presence of an additional scale k_F .

In order to estimate the magnitudes of higher-loop corrections, we first discuss an interplay between k_F and Λ that plays an important role for $m > 1$. Suppose $k = (\mathbf{K}, k_{d-m}, \mathbf{L}_{(k)})$ denotes the momentum that flows through a boson propagator within a two-loop or higher-loop diagram. When $|\mathbf{K}|$ is order of Λ , the typical momentum carried by a boson along the tangential direction of the Fermi surface is given by

$$|\mathbf{L}_{(k)}|^3 \sim \tilde{\alpha} \Lambda^{d-m}, \quad (24)$$

where

$$\tilde{\alpha} = \beta_d e^2 \mu^x (\mu \tilde{k}_F)^{\frac{m-1}{2}}. \quad (25)$$

This can be seen from the form of the boson propagator, which is given in Eq. (7). If $(\tilde{\alpha} \Lambda^{d-m})^{1/3} \gg \Lambda^{1/2}$, the momentum imparted from the boson to fermion is much larger than $\Lambda^{1/2}$ as is illustrated in Fig. 6. In this case, the typical energy of virtual particle-hole excitations within the loop is much larger than Λ . As a result, the loop contributions are suppressed by a power of Λ/k_F at low energies. On the other hand, there is no such suppression if $(\tilde{\alpha} \Lambda^{d-m})^{1/3} \ll \Lambda^{1/2}$. The crossover is controlled by the dimensionless quantity,

$$\lambda_{\text{cross}} \equiv \tilde{e}^2 \left(\frac{k_F}{\Lambda} \right)^{m-1}, \quad (26)$$

which determines whether $(\tilde{\alpha} \Lambda^{d-m})^{1/3} \gg \Lambda^{1/2}$ or $(\tilde{\alpha} \Lambda^{d-m})^{1/3} \ll \Lambda^{1/2}$.

For $m = 1$, k_F -dependence drops out from everywhere. Since $\tilde{e} \sim \mathcal{O}(\epsilon)$ within the perturbative window, one always deals with the limit,

$$\lambda_{\text{cross}} \ll 1, \quad \text{for } m = 1. \quad (27)$$

The situation is different for $m > 1$. Unlike the case with $m = 1$, the tangential momentum carried by the boson depends on both Λ and k_F . For a fixed value of $\tilde{e} \sim \mathcal{O}(\epsilon)$, one is always in the limit of

$$\lambda_{\text{cross}} \gg 1, \quad \text{for } m > 1, \quad (28)$$

at sufficiently low energies. This is because k_F has a positive scaling dimension, and k_F/Λ flows to ∞ in the low-energy limit. The crossover occurs at the energy scale $\Lambda \sim \tilde{e}^{\frac{2}{m-1}} k_F$. It is noted that there exists a large energy window for small ϵ and $(m-1)$, before the theory enters into the low-energy limit controlled by $\lambda_{\text{cross}} \gg 1$. There can be non-trivial quantum corrections from higher-loop diagrams in this intermediate energy scale. We postpone the detailed study of the intermediate scale to a future work. Here we focus on the low-energy limit with $\lambda_{\text{cross}} \gg 1$. In this limit, higher-loop diagrams are suppressed by k_F as was shown in an earlier work⁴⁶, for the special case of $m = 2$ in three dimensions.

For general $m > 1$ with $\lambda_{\text{cross}} \gg 1$, the two-loop self-energies for boson and fermion are given by

$$\Pi_2(q) \sim \frac{\tilde{e}^{\frac{m}{m+1}}}{k_F^{\frac{m-1}{2(m+1)}}} \frac{|\mathbf{Q}|^{\frac{m}{m+1}}}{N |\mathbf{L}(q)|} \Pi_1(q), \quad (29)$$

$$\Sigma_{2a}(q) \sim \tilde{e}^{\frac{2(m-1)}{m+1}} \left(\frac{\Lambda}{k_F} \right)^{\frac{2(m-1)}{m+1}} i \gamma_{d-m} \delta_q, \quad (30)$$

$$\Sigma_{2b}(q) \sim \tilde{e}^{\frac{2m}{m+1}} \left(\frac{\Lambda}{k_F} \right)^{\frac{m-1}{m+1}} \frac{i \mathbf{\Gamma} \cdot \mathbf{Q}}{N^2} \quad (31)$$

to the leading order in Λ/k_F . See Appendix B for the derivation of the results. Here $\Pi_2(q)$ is the two-loop boson self-energy contributed from Fig. 7(a). $\Sigma_{2a}(q)$ and $\Sigma_{2b}(q)$ are the fermion self-energy from Fig. 8(a), which are proportional to $\gamma_{d-m} \delta_q$ and $(\mathbf{\Gamma} \cdot \mathbf{Q})$ respectively. Other diagrams in Figs. 7(b)-(e) and 8(b)-(c) do not contribute¹⁸. The coefficients in the expressions for $\Sigma_{2a,2b}(q)$ vanish at $d-m=1$. The vertex correction is related to the fermion self-energy through the Ward identity.

Compared to the one-loop self-energies, the two-loop corrections are suppressed not only by \tilde{e} but also by powers of Λ/k_F . Because of the suppression by $1/k_F$, there is no logarithmic or higher-order divergence at the critical dimension. As a result, the critical exponents are not modified by the two-loop diagrams in the $k_F \rightarrow \infty$ limit. It is noted that the suppression by Λ/k_F originates

from the large Landau damping which suppresses quantum fluctuations at low energies. Since the suppression is not specific to the two-loop diagrams, we expect that all higher-loop diagrams are also suppressed by \tilde{e} and $1/k_F$ in the low-energy limit. We have checked this explicitly for some three-loop diagrams.

VII. CONCLUSION

To summarize, we have extracted the scaling behaviour of non-Fermi liquids with a Fermi surface of general dimensions and co-dimensions based on a dimensional regularization scheme. For $m > 1$, the low-energy physics becomes sensitive to the size of Fermi surface k_F , which results in UV/IR mixing. As a result, the upper critical dimension is shifted from the one predicted by the power-counting, and the perturbative expansion is controlled by a combination of the Yukawa coupling and the Fermi momentum k_F . By tuning the dimension below the upper critical dimension, we have shown that there exists a stable non-Fermi liquid fixed point where both interaction and UV/IR mixing play crucial roles. We have also shown that the critical exponents at the low-energy fixed point are not modified by the two-loop diagrams, due to the UV/IR mixing for $m > 1$. This is likely to be

the case for all higher-loop diagrams as well.

So far we have not considered the four-fermion interaction V , which has the tree-level scaling dimension $-d+1+m/2$. However, scatterings in the pairing channel are enhanced by the volume of the Fermi surface $\sim k_F^{m/2}$. As a result, the effective coupling that dictates the potential instability, driven by the four-fermion interactions, is given by $\tilde{V} = V k_F^{m/2}$, which has an enhanced scaling dimension $-d+1+m$. \tilde{V} is marginal at the tree-level for co-dimension $d-m=1$. For a co-dimension $d-m > 1$, there is no perturbative pairing instability for a sufficiently small $\epsilon = d_c - d$. When $d-m-1 \lesssim \epsilon$ with $d_c - d \sim \epsilon$, the interaction plays an important role for the pairing instability^{47,48}.

ACKNOWLEDGMENTS

We thank Ganapathy Baskaran, Liam Fitzpatrick, Shamit Kachru, Max Metlitski, Sri Raghu, and Subir Sachdev for stimulating discussions. The research was supported by NSERC, ERA and the Templeton Foundation. Research at the Perimeter Institute is supported in part by the Government of Canada through Industry Canada, and by the Province of Ontario through the Ministry of Research and Information.

-
- ¹ T. Holstein, R. E. Norton and P. Pincus, Phys. Rev. B **8**, 2649 (1973).
 - ² M. Y. Reizer, Phys. Rev. B **40**, 11571 (1989).
 - ³ P. A. Lee and N. Nagaosa, Phys. Rev. B **46**, 5621 (1992).
 - ⁴ B. I. Halperin, P. A. Lee and N. Read, Phys. Rev. B **47**, 7312 (1993).
 - ⁵ J. Polchinski, Nucl. Phys. B **422**, 617 (1994).
 - ⁶ B. L. Altshuler, L. B. Ioffe and A. J. Millis, Phys. Rev. B **50**, 14048 (1994).
 - ⁷ Y. B. Kim, A. Furusaki, X.-G. Wen and P. A. Lee, Phys. Rev. B **50**, 17917 (1994).
 - ⁸ C. Nayak and F. Wilczek, Nucl. Phys. B **417**, 359 (1994); Nucl. Phys. B **430**, 534 (1994).
 - ⁹ S.-S. Lee, Phys. Rev. B **80**, 165102 (2009).
 - ¹⁰ S. Sur and S.-S. Lee, Phys. Rev. B **90**, 045121 (2014).
 - ¹¹ M. A. Metlitski and S. Sachdev, Phys. Rev. B **82**, 075127 (2010).
 - ¹² M. A. Metlitski and S. Sachdev, Phys. Rev. B **82**, 075128 (2010).
 - ¹³ M. J. Lawler, D. G. Barci, V. Fernandez, E. Fradkin, and L. Oxman, Phys. Rev. B **73**, 085101 (2006); M. J. Lawler and E. Fradkin, Phys. Rev. B **75**, 033304 (2007).
 - ¹⁴ A. Abanov, A. V. Chubukov and J. Schmalian, Advances in Physics **52**, 119-218 (2003).
 - ¹⁵ A. Abanov, A. V. Chubukov, Phys. Rev. Lett. **84**, 5608 (2000); *ibid.* **93**, 255702 (2004).
 - ¹⁶ D.F. Mross, J. McGreevy, H. Liu, and T. Senthil, Phys. Rev. B **82**, 045121 (2010).
 - ¹⁷ H.-C. Jiang, M. S. Block, R. V. Mishmash, J. R. Garrison, D. N. Sheng, O. I. Motrunich and M. P. A. Fisher, Nature **493**, 39 (2013).
 - ¹⁸ D. Dalidovich and S.-S. Lee, Phys. Rev. B **88**, 245106 (2013).
 - ¹⁹ S. Sur and S.-S. Lee, Phys. Rev. B **91**, 125136 (2015).
 - ²⁰ V. Oganesyan, S. A. Kivelson, and E. Fradkin, Phys. Rev. B **64**, 195109 (2001).
 - ²¹ W. Metzner, D. Rohe, and S. Andergassen, Phys. Rev. Lett. **91**, 066402 (2003);
 - ²² L. Dell'Anna and W. Metzner, Phys. Rev. B **73**, 045127 (2006); Phys. Rev. Lett. **98**, 136402 (2007).
 - ²³ H.-Y. Kee, E. H. Kim, and C.-H. Chung, Phys. Rev. B **68**, 245109 (2003).
 - ²⁴ J. Rech, C. P  pin, and A. V. Chubukov, Phys. Rev. B **74**, 195126 (2006).
 - ²⁵ P. W  lfle and A. Rosch, J. Low Temp. Phys. **147**, 165 (2007).
 - ²⁶ D.L. Maslov and A.V. Chubukov, Phys. Rev. B **81**, 045110 (2010).
 - ²⁷ J. Quintanilla and A. J. Schofield, Phys. Rev. B **74**, 115126.
 - ²⁸ H. Yamase and H. Kohno, J. Phys. Soc. Jpn. **69**, 2151 (2000).
 - ²⁹ H. Yamase, V. Oganesyan, and W. Metzner, Phys. Rev. B **72**, 035114 (2005).
 - ³⁰ C. J. Halboth and W. Metzner, Phys. Rev. Lett. **85**, 5162 (2000).
 - ³¹ P. Jakubczyk, P. Strack, A. A. Katanin, and W. Metzner, Phys. Rev. B **77**, 195120 (2008).
 - ³² M. Zacharias, P. W  lfle, and M. Garst, Phys. Rev. B **80**, 165116 (2009).

- ³³ E.-A. Kim, M.J. Lawler, P. Oreto, S. Sachdev, E. Fradkin, and S. A. Kivelson, Phys. Rev. B **77**, 184514 (2008).
³⁴ Y. Huh and S. Sachdev, Phys. Rev. B **78**, 064512 (2008).
³⁵ O. I. Motrunich, Phys. Rev. B **72**, 045105 (2005).
³⁶ S.-S. Lee and P. A. Lee, Phys. Rev. Lett. **95**, 036403 (2005).
³⁷ P. A. Lee, N. Nagaosa and X.-G. Wen, Rev. Mod. Phys. **78**, 17 (2006); references therein.
³⁸ O. I. Motrunich and M. P. A. Fisher, Phys. Rev. B **75**, 235116 (2007).
³⁹ T. Senthil, Phys. Rev. B **78**, 035103 (2008).
⁴⁰ S.-S. Lee, Phys. Rev. B **78**, 085129 (2008).
⁴¹ If there is a superconducting instability, the locality in momentum space breaks down even for $m = 1$. Here we assume $d - m > 1$, for which there is no perturbative pairing instability.
⁴² A. L. Fitzpatrick, S. Kachru, J. Kaplan and S. Raghu, Phys. Rev. B **88**, 125116 (2013); *ibid.* **89**, 165114 (2014); R. Mahajan, D.M. Ramirez, S. Kachru, S. Raghu, arXiv:1303.1587.
⁴³ G. Torroba and H. Wang, arXiv:1406.3029.
⁴⁴ S. Chakravarty, R. E. Norton, and O. F. Syljuåsen, Phys. Rev. Lett., **74**, 1423 (1995).
⁴⁵ T. Senthil and R. Shankar, Phys. Rev. Lett. **102**, 046406 (2009).
⁴⁶ T. Schäfer and K. Schwenzer, Phys. Rev.D **70**, 054007 (2004).
⁴⁷ M. A. Metlitski, D. F. Mross, S. Sachdev, T. Senthil, Phys.Rev.B **91**, 115111 (2015).
⁴⁸ I. Mandal and S.-S. Lee, in progress.

Appendix A: Computation of the Feynman Diagrams at One-loop

1. One-loop boson self-energy

In this section, we compute the one-loop boson self-energy :

$$\Pi_1(q) = -(ie)^2 \mu^x \int dk \text{Tr} [\gamma_{d-m} G_0(k+q) \gamma_{d-m} G_0(k)] , \quad (\text{A1})$$

where the bare fermion propagator is given by $G_0(k) = \frac{1}{i} \frac{\mathbf{\Gamma} \cdot \mathbf{K} + \gamma_{d-m} \delta_k}{\mathbf{K}^2 + \delta_k^2} \exp \left\{ -\frac{\mathbf{L}_{(k)}^2}{\mu k_F} \right\}$. Performing the integration over k_{d-m} , we obtain

$$\Pi_1(q) = e^2 \mu^x \int \frac{d\mathbf{L}_{(k)} d\mathbf{K}}{(2\pi)^d} \frac{(|\mathbf{K} + \mathbf{Q}| + |\mathbf{K}|) [\mathbf{K} \cdot (\mathbf{K} + \mathbf{Q}) - |\mathbf{K}| |\mathbf{K} + \mathbf{Q}|] \exp \left(-\frac{\mathbf{L}_{(k)}^2 + \mathbf{L}_{(k+q)}^2}{\mu k_F} \right)}{|\mathbf{K}| |\mathbf{K} + \mathbf{Q}| \left[(\delta_q + 2 q_{d-m+1} k_{d-m+1})^2 + (|\mathbf{K} + \mathbf{Q}| + |\mathbf{K}|)^2 \right]} ,$$

where we have chosen a coordinate system such that $\mathbf{L}_{(q)} = (q_{d-m+1}, 0, 0, \dots, 0)$, without loss of generality. Because of the rotational symmetry in $\mathbf{L}_{(q)}$, $\Pi_1(q)$ depends only on its magnitude. From the expression for the integration over k_{d-m+1} ,

$$\begin{aligned} I &\equiv \int \frac{dk_{d-m+1}}{2\pi} \frac{\exp \left[-\frac{2 k_{d-m+1} (k_{d-m+1} + |\mathbf{L}_{(q)}|) + |\mathbf{L}_{(q)}|^2}{k_F} \right]}{(\delta_q + 2 k_{d-m+1} |\mathbf{L}_{(q)}|)^2 + (|\mathbf{K} + \mathbf{Q}| + |\mathbf{K}|)^2} \\ &= \exp \left(-\frac{|\mathbf{L}_{(q)}|^2}{2k_F} \right) \frac{1}{|\mathbf{L}_{(q)}|^2 \sqrt{8 k_F}} \times \mathcal{F} \left(\frac{|\mathbf{K} + \mathbf{Q}| + |\mathbf{K}|}{|\mathbf{L}_{(q)}| \sqrt{2 k_F}}, \frac{q_{d-m}}{|\mathbf{L}_{(q)}| \sqrt{2 k_F}} \right) , \end{aligned} \quad (\text{A2})$$

with

$$\mathcal{F}(y, u) = \int_{-\infty}^{\infty} \frac{dz}{2\pi} \frac{\exp(-z^2)}{(z+u)^2 + y^2} , \quad (\text{A3})$$

and $J \equiv \int_{-\infty}^{\infty} \frac{dz}{2\pi} \exp \left(-\frac{2z^2}{\mu k_F} \right) = \sqrt{\frac{\mu k_F}{8\pi}}$ for the integration over the remaining components of $\mathbf{L}_{(k)}$, the self-energy is written as:

$$\Pi_1(q) = \frac{e^2 \mu^x J^{m-1} \exp \left(-\frac{|\mathbf{L}_{(q)}|^2}{2k_F} \right)}{|\mathbf{L}_{(q)}|^2 \sqrt{8 k_F} (2\pi)^{d-m}} \int d\mathbf{K} \left\{ \frac{\mathbf{K} \cdot (\mathbf{K} + \mathbf{Q})}{|\mathbf{K}| |\mathbf{K} + \mathbf{Q}|} - 1 \right\} (|\mathbf{K} + \mathbf{Q}| + |\mathbf{K}|) \mathcal{F} \left(\frac{|\mathbf{K} + \mathbf{Q}| + |\mathbf{K}|}{|\mathbf{L}_{(q)}| \sqrt{2 k_F}}, \frac{q_{d-m}}{|\mathbf{L}_{(q)}| \sqrt{2 k_F}} \right) . \quad (\text{A4})$$

It is difficult to obtain the exact expression of $\Pi_1(q)$ for general values of k_F and q . Here we focus on the limit of physical importance where k_F is much larger than all other scales, including external momentum and the UV cut-off of \mathbf{K} . In this limit, we use $\mathcal{F}(y, u) \simeq \frac{1}{2|y|}$ for $y, u \ll 1$ to simplify the expression for the self-energy to

$$\Pi_1(q) = \frac{e^2 \mu^x}{2^{m+1} |\mathbf{L}_{(q)}|} \left(\frac{\mu \tilde{k}_F}{2\pi} \right)^{\frac{m-1}{2}} I_1(d-m, \mathbf{Q}), \quad (\text{A5})$$

where

$$I_1(d-m, \mathbf{Q}) = \int \frac{d\mathbf{K}}{(2\pi)^{d-m}} \left\{ \frac{\mathbf{K} \cdot (\mathbf{K} + \mathbf{Q})}{|\mathbf{K}| |\mathbf{K} + \mathbf{Q}|} - 1 \right\}. \quad (\text{A6})$$

Using the Feynman parametrization

$$\frac{1}{A^{n_1} B^{n_2}} = \frac{\Gamma(n_1 + n_2)}{\Gamma(n_1) \Gamma(n_2)} \int_0^1 \frac{t^{n_1-1} (1-t)^{n_2-1} dt}{[tA + (1-t)B]^{n_1+n_2}}, \quad (\text{A7})$$

with $n_1 = n_2 = 1/2$, $A = |\mathbf{K} + \mathbf{Q}|^2$ and $B = |\mathbf{K}|^2$ we rewrite Eq. (A6) as

$$I_1(d-m, \mathbf{Q}) = \frac{1}{\pi (2\pi)^{d-m}} \int_0^1 \frac{dt}{\sqrt{t(1-t)}} \int d\mathbf{K} \left\{ \frac{\mathbf{K} \cdot (\mathbf{K} + \mathbf{Q})}{t|\mathbf{K} + \mathbf{Q}|^2 + (1-t)\mathbf{K}^2} - 1 \right\}.$$

The integrations over \mathbf{K} and t give

$$I_1(d-m, \mathbf{Q}) = -\frac{\Gamma^2(\frac{d-m+1}{2}) |\mathbf{Q}|^{d-m}}{2^{d-m-1} \pi^{\frac{d-m}{2}} \Gamma(\frac{d-m}{2}) \Gamma(d-m+1) |\cos\{\frac{\pi(d-m+1)}{2}\}|}, \quad (\text{A8})$$

for $0 < d-m < 2$, and the self-energy is obtained to be

$$\Pi_1(q) = -\beta_d e^2 \mu^x \frac{|\mathbf{Q}|^{d-m} (\mu \tilde{k}_F)^{\frac{m-1}{2}}}{|\mathbf{L}_{(q)}|}, \quad (\text{A9})$$

where β_d is defined after Eq. (7).

The expression in Eq. (A9) is valid for $\frac{|\mathbf{Q}|}{|\mathbf{L}_{(q)}| \sqrt{k_F}} \ll 1$ and $\frac{q_{d-m}}{|\mathbf{L}_{(q)}| \sqrt{k_F}} \ll 1$. On the other hand, it is no longer valid in a slim region of q satisfying $\frac{|\mathbf{Q}|}{|\mathbf{L}_{(q)}| \sqrt{k_F}} \gg 1$ or $\frac{q_{d-m}}{|\mathbf{L}_{(q)}| \sqrt{k_F}} \gg 1$, when k_F is large but finite. Now let us consider the boson self-energy in this region. When $\frac{|\mathbf{Q}|}{|\mathbf{L}_{(q)}| \sqrt{k_F}} \gg 1$ or $\frac{q_{d-m}}{|\mathbf{L}_{(q)}| \sqrt{k_F}} \gg 1$, we need to use the expression

$$\mathcal{F}(y, u) \simeq \frac{1}{y^2 + u^2} \int_{-\infty}^{\infty} \frac{dz}{2\pi} \exp(-z^2) = \frac{1}{2\sqrt{\pi} (y^2 + u^2)} \quad (\text{A10})$$

for $u \gg 1$ or $y \gg 1$, and the self-energy becomes

$$\Pi_1(q) = \frac{e^2 \mu^x J^{m-1} \sqrt{k_F}}{(2\pi)^{d-m} \sqrt{8\pi}} (t_1 + t_2), \quad (\text{A11})$$

where

$$t_1 = \int_{|\mathbf{K}| < |\mathbf{Q}|} d\mathbf{K} T(\mathbf{K}, \mathbf{Q}, q_{d-m}), \quad (\text{A12})$$

$$t_2 = \int_{|\mathbf{K}| > |\mathbf{Q}|} d\mathbf{K} T(\mathbf{K}, \mathbf{Q}, q_{d-m}), \quad (\text{A13})$$

with $T(\mathbf{K}, \mathbf{Q}, q_{d-m}) = \left\{ \frac{\mathbf{K} \cdot (\mathbf{K} + \mathbf{Q})}{|\mathbf{K}| |\mathbf{K} + \mathbf{Q}|} - 1 \right\} \frac{|\mathbf{K} + \mathbf{Q}| + |\mathbf{K}|}{(|\mathbf{K} + \mathbf{Q}| + |\mathbf{K}|)^2 + q_{d-m}^2}$. We can estimate t_1 and t_2 as

$$t_1 \sim -\frac{|\mathbf{Q}|^{d-m+1}}{|\mathbf{Q}|^2 + q_{d-m}^2}, \quad t_2 \sim -|\mathbf{Q}|^2 |q_{d-m}|^{d-m-3} g\left(\frac{|\mathbf{Q}|}{|q_{d-m}|}\right), \quad (\text{A14})$$

where $g(t) = \int_t^\infty dv \frac{v^{d-m-2}}{1+4v^2}$. Hence, near $|\mathbf{L}_{(q)}| = 0$, the boson self-energy becomes

$$\Pi_1(q) \simeq -e^2 \mu^x J^{m-1} \sqrt{k_F} \tilde{f}(|\mathbf{Q}|, q_{d-m}), \quad (\text{A15})$$

where

$$\tilde{f}(|\mathbf{Q}|, q_{d-m}) \sim \left[\frac{|\mathbf{Q}|^{d-m+1}}{|\mathbf{Q}|^2 + q_{d-m}^2} + \tilde{C} |\mathbf{Q}|^2 |q_{d-m}|^{d-m-3} g\left(\frac{|\mathbf{Q}|}{|q_{d-m}|}\right) \right], \quad (\text{A16})$$

with $\tilde{C} > 0$, a constant. The full one-loop boson self-energy crosses over from Eq. (A9) to Eq. (A15) around $\frac{|\mathbf{Q}|}{|\mathbf{L}_{(q)}| \sqrt{k_F}}, \frac{q_{d-m}}{|\mathbf{L}_{(q)}| \sqrt{k_F}} \sim 1$. However, the range of q in which Eq. (A15) is needed becomes vanishingly small in the large k_F limit. As a result, we can use Eq. (A9) for the dressed boson propagator to the leading order in $1/k_F$ as will be shown explicitly in the next section.

2. One-loop fermion self-energy

Here we compute the one-loop fermion self-energy:

$$\Sigma_1(q) = \frac{(ie)^2 \mu^x}{N} \int dk \gamma_{d-m} G_0(q-k) \gamma_{d-m} D_1(k). \quad (\text{A17})$$

We will first compute Eq. (A17) using $D_1(k)$ dressed with the boson-self energy in Eq. (A9). Integrating over k_{d-m} , we obtain

$$\Sigma_1(q) = \frac{ie^2 \mu^x}{2N} \int \frac{d\mathbf{K}}{(2\pi)^{d-m}} \frac{\mathbf{\Gamma} \cdot (\mathbf{K} - \mathbf{Q})}{|\mathbf{K} - \mathbf{Q}|} \times I_2,$$

where

$$\begin{aligned} I_2 &= \int \frac{d\Omega_m}{(2\pi)^{m-1}} \int_0^\infty \frac{d|\mathbf{L}_{(k)}|}{2\pi} \frac{|\mathbf{L}_{(k)}|^{m-1}}{|\mathbf{L}_{(k)}|^2 - \Pi_1(k)} \\ &= \frac{(\pi)^{\frac{2-m}{2}}}{3 \times 2^{m-1} \Gamma(m/2) |\sin\{(m+1)\pi/3\}| \{\beta_d e^2 \mu^x (\mu \tilde{k}_F)^{\frac{m-1}{2}} |\mathbf{K}|^{d-m}\}^{\frac{2-m}{3}}}. \end{aligned} \quad (\text{A18})$$

Here we have assumed that $0 < m+1 < 3$, for which the $|\mathbf{L}_{(k)}|$ integral converges without the exponential damping factor in the fermion propagator. Therefore, we obtain

$$\Sigma_1(q) = \frac{ie^{2(m+1)/3} \mu^{x(m+1)/3} \pi^{(2-m)/2} \times I_3(d-m, \mathbf{Q})}{6N \times 2^{m-1} \Gamma(m/2) |\sin\{(m+1)\pi/3\}| \beta_d^{(2-m)/3} (\mu \tilde{k}_F)^{(m-1)(2-m)/6}} \quad (\text{A19})$$

to the leading order in $1/k_F$, where

$$I_3(d-m, \mathbf{Q}) = \int \frac{d\mathbf{K}}{(2\pi)^{d-m}} \frac{\mathbf{\Gamma} \cdot (\mathbf{K} - \mathbf{Q})}{|\mathbf{K}|^{(d-m)(2-m)/3} |\mathbf{K} - \mathbf{Q}|}. \quad (\text{A20})$$

Using the Feynman parametrization (A7), we obtain

$$\begin{aligned} I_3(d-m, \mathbf{Q}) &= \frac{\Gamma(\frac{1}{2} + \beta)}{\Gamma(\beta) \sqrt{\pi} (2\pi)^{d-m}} \int_0^1 \frac{dt (1-t)^{\beta-1}}{\sqrt{t}} \int d\mathbf{K} \frac{\mathbf{\Gamma} \cdot (\mathbf{K} - \mathbf{Q})}{[t|\mathbf{K} - \mathbf{Q}|^2 + (1-t)\mathbf{K}^2]^{\frac{1}{2} + \beta}} \\ &= -\frac{\Gamma(\beta - \frac{d-m-1}{2}) \Gamma(\frac{d-m-2\beta}{2}) \Gamma(\frac{d-m+1}{2}) \mathbf{\Gamma} \cdot \mathbf{Q}}{\Gamma(\beta) \Gamma(d-m-\beta + \frac{1}{2}) \sqrt{\pi} (4\pi)^{\frac{d-m}{2}} (\mathbf{Q}^2)^{\beta - \frac{d-m-1}{2}}}, \end{aligned} \quad (\text{A21})$$

where $\beta \equiv \frac{(d-m)(2-m)}{6}$. Finally, the fermion self-energy is obtained to be

$$\begin{aligned} \Sigma_1(q) &= -\frac{ie^{2(m+1)/3} \mu^{x(m+1)/3} \mathbf{\Gamma} \cdot \mathbf{Q}}{6N \pi^{(m-1)/2} (4\pi)^{\frac{d-m}{2}} 2^{m-1} |\sin\{(m+1)\pi/3\}| \beta_d^{(2-m)/3} (\mu \tilde{k}_F)^{(m-1)(2-m)/6} (\mathbf{Q}^2)^{\frac{3-(m+1)(d-m)}{6}}} \\ &\quad \times \frac{\Gamma(\frac{3-(m+1)(d-m)}{6}) \Gamma(\frac{d-m-2\beta}{2}) \Gamma(\frac{d-m+1}{2})}{\Gamma(m/2) \Gamma(\beta) \Gamma(d-m-\beta + \frac{1}{2})}. \end{aligned} \quad (\text{A22})$$

The above expression has been obtained by using the boson self-energy in Eq. (A9), which is valid in the large k_F limit. Now we explicitly check that our use of Eq. (A9) in Eq. (A17) is valid to the leading order in $1/k_F$. Suppose we use the exact expression of the one-loop boson self-energy, which is valid for all k_F , to compute the fermion self-energy:

$$\Sigma_1^{exact}(q) = \frac{i e^2 \mu^x}{N} \int dk \frac{\exp\left(-\frac{\mathbf{L}_{(q-k)}^2}{k_F}\right)}{\mathbf{L}_{(k)}^2 - \Pi_1^{exact}(k)} \frac{\gamma_{d-m} \delta_{q-k} - \mathbf{\Gamma} \cdot (\mathbf{Q} - \mathbf{K})}{(\mathbf{Q} - \mathbf{K})^2 + \delta_{q-k}^2}. \quad (\text{A23})$$

Π_1^{exact} deviates from Π_1 in Eq. (A9) for $|\mathbf{L}_{(k)}| < \delta \equiv \frac{\Lambda}{\sqrt{k_F}} \ll \sqrt{\Lambda} \ll \sqrt{k_F}$, where Λ is the UV cut-off for \mathbf{K} . In this region, we can safely ignore the exponential damping factor and the contribution of $|\mathbf{L}_{(k)}|$ in δ_{q-k} . In this case, we have

$$\begin{aligned} \Sigma_1^{exact}(q) - \Sigma_1(q) &\simeq \frac{i e^2 \mu^x}{N} \int \frac{d\mathbf{K} dk_{d-m}}{(2\pi)^{d+1}} \int_{|\mathbf{L}_{(k)}|=0}^{|\mathbf{L}_{(k)}|=\delta} d\mathbf{L}_{(k)} \frac{\gamma_{d-m} \delta_{q-k} - \mathbf{\Gamma} \cdot (\mathbf{Q} - \mathbf{K})}{(\mathbf{Q} - \mathbf{K})^2 + \delta_{q-k}^2} \left[\frac{1}{\mathbf{L}_{(k)}^2 - \Pi_1^{exact}(k)} - \frac{1}{\mathbf{L}_{(k)}^2 - \Pi_1(k)} \right] \\ &\simeq \frac{i e^2 \mu^x}{N} \int d\Omega_m \int \frac{d\mathbf{K} dk_{d-m}}{(2\pi)^{d+1}} \left[\frac{\gamma_{d-m} \delta_{q-k} - \mathbf{\Gamma} \cdot (\mathbf{Q} - \mathbf{K})}{(\mathbf{Q} - \mathbf{K})^2 + \delta_{q-k}^2} \right] \Big|_{|\mathbf{L}_{(k)}|=0} (i_{21} - i_{22}), \end{aligned} \quad (\text{A24})$$

where

$$i_{21} = \int_{|\mathbf{L}_{(k)}|=0}^{|\mathbf{L}_{(k)}|=\delta} \frac{d|\mathbf{L}_{(k)}| |\mathbf{L}_{(k)}|^{m-1}}{\mathbf{L}_{(k)}^2 + e^2 \mu^x J^{m-1} \sqrt{k_F} \tilde{f}(|\mathbf{K}|, k_{d-m})}, \quad i_{22} = \int_{|\mathbf{L}_{(k)}|=0}^{|\mathbf{L}_{(k)}|=\delta} \frac{d|\mathbf{L}_{(k)}| |\mathbf{L}_{(k)}|^{m-1}}{\mathbf{L}_{(k)}^2 - \Pi_1(k)}. \quad (\text{A25})$$

Integrating over $|\mathbf{L}_{(k)}|$, we obtain

$$i_{21} = {}_2F_1\left(1, \frac{m}{2}; \frac{m+2}{2}; -\frac{\delta^2}{e^2 \mu^x J^{m-1} \sqrt{k_F} \tilde{f}(|\mathbf{K}|, k_{d-m})}\right) \frac{\delta^m}{m e^2 \mu^x J^{m-1} \sqrt{k_F} \tilde{f}(|\mathbf{K}|, k_{d-m})}, \quad (\text{A26})$$

$$i_{22} = {}_2F_1\left(1, \frac{m+1}{3}; \frac{m+4}{3}; -\frac{\delta^3}{\beta_d e^2 \mu^x k_F^{\frac{m-1}{2}} |\mathbf{K}|^{(d-m)}}\right) \frac{\delta^{m+1}}{(m+1) \beta_d e^2 \mu^x k_F^{\frac{m-1}{2}} |\mathbf{K}|^{(d-m)}}, \quad (\text{A27})$$

where ${}_2F_1$ is the hypergeometric function. In the limit $k_F \rightarrow \infty$ with fixed Λ , we have $\frac{i_{21}}{I_2}, \frac{i_{22}}{I_2} \sim k_F^{-\frac{m^2-m+2}{2}} \rightarrow 0$, where I_2 is defined in Eq. (A18). Therefore, $\Sigma^{exact}(q)$ goes to $\Sigma(q)$ in the large k_F limit, and Eq. (A22) is valid to the leading order in $1/k_F$.

Appendix B: Computation of the Feynman Diagrams at Two-loop

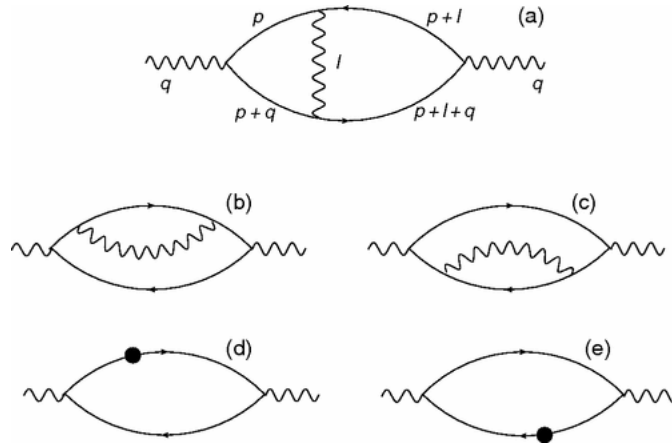


FIG. 7. The diagrams for two-loop boson self-energy.

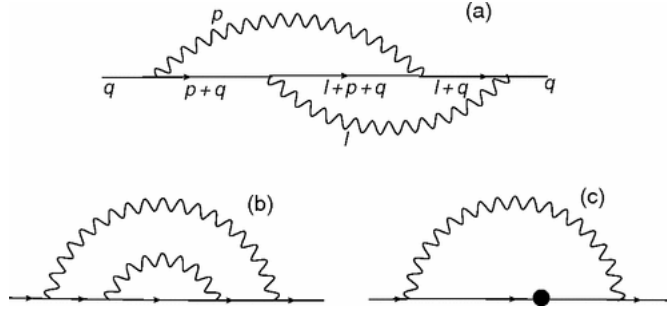


FIG. 8. The diagrams for two-loop fermion self-energy.

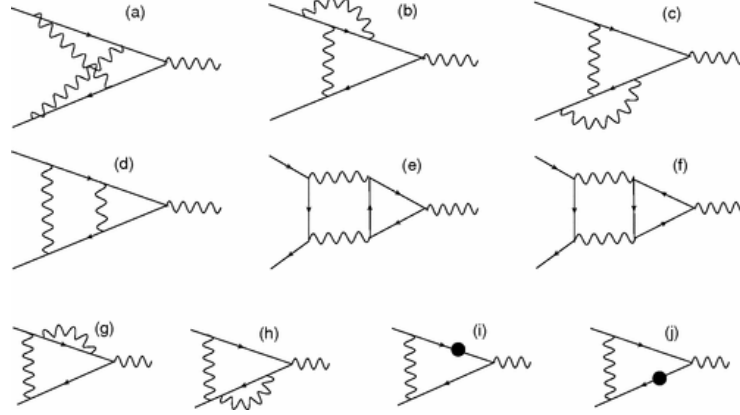


FIG. 9. The diagrams for two-loop vertex corrections.

All the two-loop diagrams are shown in Figs. 7,8 and 9. The black circles in Figs. 7 (d)-(e), 8(c) and 9(i)-(j) denote the one-loop counterterm for the fermion self-energy,

$$i A_1^{(1)} \bar{\Psi}(\mathbf{\Gamma} \cdot \mathbf{Q}) \Psi. \quad (\text{B1})$$

Among the self-energy diagrams, only Figs. 7(a) and 8(a) contribute¹⁸. The vertex correction can be obtained from the fermion self-energy correction through the Ward identity. As we will see through explicit computations in the following sections, the two-loop diagrams are suppressed not only by \tilde{e} but also by Λ/k_F in the low-energy limit for $m > 1$.

1. Two-loop contribution to boson self-energy

We compute the two-loop boson self-energy shown in Fig. 7 (a):

$$\Pi_2(q) = -\frac{e^4 \mu^{2x} N}{N^2} \int dl dp D_1(l) \text{Tr}\{\gamma_{d-m} G_0(p) \gamma_{d-m} G_0(p+l) \gamma_{d-m} G_0(p+l+q) \gamma_{d-m} G_0(p+q)\}. \quad (\text{B2})$$

Taking the trace, we obtain

$$\Pi_2(q) = -\frac{e^4 \mu^{2x}}{N} \int dl dp D_1(l) \frac{\mathcal{B}_1}{\mathcal{D}_1} \exp\left(-\frac{\mathbf{L}_{(p)}^2 + \mathbf{L}_{(p+q)}^2 + \mathbf{L}_{(p+l)}^2 + \mathbf{L}_{(p+l+q)}^2}{k_F}\right), \quad (\text{B3})$$

where

$$\begin{aligned} \mathcal{B}_1 &= 2[\delta_{p+l} \delta_{p+q+l} - (\mathbf{P} + \mathbf{L}) \cdot (\mathbf{P} + \mathbf{L} + \mathbf{Q})][\delta_{p+q} \delta_p - (\mathbf{P} + \mathbf{Q}) \cdot \mathbf{P}] - 2[(\mathbf{P} + \mathbf{L}) \cdot (\mathbf{P} + \mathbf{Q})][(\mathbf{P} + \mathbf{L} + \mathbf{Q}) \cdot \mathbf{P}] \\ &\quad + 2[(\mathbf{P} + \mathbf{L}) \cdot \mathbf{P}][(\mathbf{P} + \mathbf{L} + \mathbf{Q}) \cdot (\mathbf{P} + \mathbf{Q})] - 2[\delta_{p+l} (\mathbf{P} + \mathbf{L} + \mathbf{Q}) + \delta_{p+l+q} (\mathbf{P} + \mathbf{L})] \cdot [\delta_{p+q} \mathbf{P} + \delta_p (\mathbf{P} + \mathbf{Q})], \\ \mathcal{D}_1 &= [\delta_p^2 + \mathbf{P}^2][\delta_{p+q}^2 + (\mathbf{P} + \mathbf{Q})^2][\delta_{p+l}^2 + (\mathbf{P} + \mathbf{L})^2][\delta_{p+l+q}^2 + (\mathbf{P} + \mathbf{L} + \mathbf{Q})^2]. \end{aligned} \quad (\text{B4})$$

Shifting the variables as

$$p_{d-m} \rightarrow p_{d-m} - \mathbf{L}_{(p)}^2, \quad l_{d-m} \rightarrow l_{d-m} - p_{d-m} - \mathbf{L}_{(p+l)}^2,$$

we can substitute

$$\delta_p \rightarrow p_{d-m}, \quad \delta_{p+q} \rightarrow p_{d-m} + 2 \mathbf{L}_{(p)} \cdot \mathbf{L}_{(q)} + \delta_q, \quad \delta_{l+p} \rightarrow l_{d-m}, \quad \delta_{p+l+q} \rightarrow l_{d-m} + 2 \mathbf{L}_{(p+l)} \cdot \mathbf{L}_{(q)} + \delta_q.$$

Integration over p_{d-m} and l_{d-m} gives us

$$\Pi_2(q) = -\frac{e^4 \mu^{2x}}{N} \int \frac{d\mathbf{L}_{(l)} d\mathbf{L} d\mathbf{L}_{(p)} d\mathbf{P}}{(2\pi)^{2d}} D_1(l) \frac{\mathcal{B}_2}{\mathcal{D}_2} \exp\left(-\frac{\mathbf{L}_{(p)}^2 + \mathbf{L}_{(p+q)}^2 + \mathbf{L}_{(p+l)}^2 + \mathbf{L}_{(p+l+q)}^2}{k_F}\right), \quad (\text{B5})$$

where

$$\begin{aligned} \mathcal{B}_2 &= 2 (|\mathbf{P} + \mathbf{L}| + |\mathbf{P} + \mathbf{L} + \mathbf{Q}|) (|\mathbf{P} + \mathbf{Q}| + |\mathbf{P}|) \\ &\times \left\{ [|\mathbf{P} + \mathbf{L}| |\mathbf{P} + \mathbf{L} + \mathbf{Q}| - (\mathbf{P} + \mathbf{L}) \cdot (\mathbf{P} + \mathbf{L} + \mathbf{Q})] [|\mathbf{P} + \mathbf{Q}| |\mathbf{P}| - (\mathbf{P} + \mathbf{Q}) \cdot \mathbf{P}] \right. \\ &\quad \left. - [(\mathbf{P} + \mathbf{L}) \cdot (\mathbf{P} + \mathbf{Q})] [(\mathbf{P} + \mathbf{L} + \mathbf{Q}) \cdot \mathbf{P}] + [(\mathbf{P} + \mathbf{L}) \cdot \mathbf{P}] [(\mathbf{P} + \mathbf{L} + \mathbf{Q}) \cdot (\mathbf{P} + \mathbf{Q})] \right\} \\ &- 2 (2 \mathbf{L}_{(p+l)} \cdot \mathbf{L}_{(q)} + \delta_q) (2 \mathbf{L}_{(p)} \cdot \mathbf{L}_{(q)} + \delta_q) \\ &\times [|\mathbf{P} + \mathbf{L} + \mathbf{Q}| (\mathbf{P} + \mathbf{L}) - |\mathbf{P} + \mathbf{L}| (\mathbf{P} + \mathbf{L} + \mathbf{Q})] \cdot [|\mathbf{P} + \mathbf{Q}| \mathbf{P} - |\mathbf{P}| (\mathbf{P} + \mathbf{Q})], \end{aligned} \quad (\text{B6})$$

$$\begin{aligned} \mathcal{D}_2 &= 4 |\mathbf{P}| |\mathbf{P} + \mathbf{Q}| |\mathbf{P} + \mathbf{L}| |\mathbf{P} + \mathbf{Q} + \mathbf{L}| \left[(2 \mathbf{L}_{(p+l)} \cdot \mathbf{L}_{(q)} + \delta_q)^2 + (|\mathbf{P} + \mathbf{L}| + |\mathbf{P} + \mathbf{Q} + \mathbf{L}|)^2 \right] \\ &\times \left[(2 \mathbf{L}_{(p)} \cdot \mathbf{L}_{(q)} + \delta_q)^2 + (|\mathbf{P}| + |\mathbf{P} + \mathbf{Q}|)^2 \right]. \end{aligned} \quad (\text{B7})$$

Without loss of generality, we can choose the coordinate system such that $\mathbf{L}_{(q)} = (q_{d-m+1}, 0, 0, \dots, 0)$ with $q_{d-m+1} > 0$. After making a further change of variables as

$$\mathbf{L} \rightarrow \mathbf{L} - \mathbf{P}, \quad \mathbf{P} \rightarrow \mathbf{P} - \frac{\mathbf{Q}}{2}, \quad 2 |\mathbf{L}_{(q)}| p_{d-m+1} + \delta_q \rightarrow p_{d-m+1}, \quad (\text{B8})$$

and integrating over p_{d-m+1} (neglecting the corresponding exponential damping part), we obtain:

$$\begin{aligned} \Pi_2(q) &\simeq -\frac{e^4 \mu^{2x}}{N} \int \frac{d\mathbf{L}_{(l)} d\mathbf{L} d\mathbf{u}_{(p)} d\mathbf{P}}{(2\pi)^d (2\pi)^{d-1}} D_1(\mathbf{L}_{(l)}, |\mathbf{L} - \mathbf{P}|) \frac{\mathcal{B}_3(\mathbf{L}, \mathbf{P}, \mathbf{Q})}{\mathcal{D}_3(l, \mathbf{P}, q)} \exp\left(-\frac{3 \mathbf{u}_{(p)}^2}{k_F}\right) \\ &\simeq -\frac{e^4 \mu^{2x}}{N} \left(\frac{k_F}{12\pi}\right)^{\frac{m-1}{2}} \int \frac{d\mathbf{L}_{(l)} d\mathbf{L}}{(2\pi)^d} \frac{d\mathbf{P}}{(2\pi)^{d-m}} D_1(\mathbf{L}_{(l)}, |\mathbf{L} - \mathbf{P}|) \frac{\mathcal{B}_3(\mathbf{L}, \mathbf{P}, \mathbf{Q})}{\mathcal{D}_3(l, \mathbf{P}, q)}, \end{aligned} \quad (\text{B9})$$

where

$$\begin{aligned} \mathbf{u}_{(k)} &= (k_{d-m+2}, \dots, k_d), \\ \mathcal{B}_3(\mathbf{L}, \mathbf{P}, \mathbf{Q}) &= \mathcal{B}_4(\mathbf{L}, \mathbf{P}, \mathbf{Q}) \bar{\mathcal{D}}(\mathbf{L}, \mathbf{P}, \mathbf{Q}), \end{aligned} \quad (\text{B10})$$

$$\begin{aligned} \mathcal{D}_3(l, \mathbf{P}, q) &= 8 |\mathbf{L}_{(q)}| \mathcal{D}_4(\mathbf{L}, \mathbf{P}, \mathbf{Q}) \left\{ \bar{\mathcal{D}}^2(\mathbf{L}, \mathbf{P}, \mathbf{Q}) + 4 (\mathbf{L}_{(q)} \cdot \mathbf{L}_{(l)})^2 \right\}, \\ \mathcal{B}_4(\mathbf{L}, \mathbf{P}, \mathbf{Q}) &= (|\mathbf{L} - \mathbf{Q}/2| |\mathbf{L} + \mathbf{Q}/2| - \mathbf{L}^2 + \mathbf{Q}^2/4) (|\mathbf{P} - \mathbf{Q}/2| |\mathbf{P} + \mathbf{Q}/2| - \mathbf{P}^2 + \mathbf{Q}^2/4) \\ &\quad - [(\mathbf{L} - \mathbf{Q}/2) \cdot (\mathbf{P} + \mathbf{Q}/2)] [(\mathbf{L} + \mathbf{Q}/2) \cdot (\mathbf{P} - \mathbf{Q}/2)] \\ &\quad + [(\mathbf{L} - \mathbf{Q}/2) \cdot (\mathbf{P} - \mathbf{Q}/2)] [(\mathbf{L} + \mathbf{Q}/2) \cdot (\mathbf{P} + \mathbf{Q}/2)] \\ &\quad - |\mathbf{L} + \mathbf{Q}/2| |\mathbf{P} + \mathbf{Q}/2| [(\mathbf{L} - \mathbf{Q}/2) \cdot (\mathbf{P} - \mathbf{Q}/2)] \\ &\quad + |\mathbf{L} + \mathbf{Q}/2| |\mathbf{P} - \mathbf{Q}/2| [(\mathbf{L} - \mathbf{Q}/2) \cdot (\mathbf{P} + \mathbf{Q}/2)] \\ &\quad + |\mathbf{L} - \mathbf{Q}/2| |\mathbf{P} + \mathbf{Q}/2| [(\mathbf{L} + \mathbf{Q}/2) \cdot (\mathbf{P} - \mathbf{Q}/2)] \\ &\quad - |\mathbf{L} - \mathbf{Q}/2| |\mathbf{P} - \mathbf{Q}/2| [(\mathbf{L} + \mathbf{Q}/2) \cdot (\mathbf{P} + \mathbf{Q}/2)], \end{aligned} \quad (\text{B11})$$

$$\mathcal{D}_4(\mathbf{L}, \mathbf{P}, \mathbf{Q}) = |\mathbf{L} - \mathbf{Q}/2| |\mathbf{L} + \mathbf{Q}/2| |\mathbf{P} - \mathbf{Q}/2| |\mathbf{P} + \mathbf{Q}/2|, \quad (\text{B12})$$

$$\bar{\mathcal{D}}(\mathbf{L}, \mathbf{P}, \mathbf{Q}) = |\mathbf{L} - \mathbf{Q}/2| + |\mathbf{L} + \mathbf{Q}/2| + |\mathbf{P} - \mathbf{Q}/2| + |\mathbf{P} + \mathbf{Q}/2|. \quad (\text{B13})$$

Note that we can ignore the exponential damping part for $\mathbf{L}_{(l)}$.

For $m > 1$ and $\lambda_{\text{cross}} \gg 1$, the angular integrals along the Fermi surface directions give a factor proportional to

$$\int_0^\pi d\theta \frac{\bar{\mathcal{D}}(\mathbf{L}, \mathbf{P}, \mathbf{Q}) \sin^{m-2} \theta}{\bar{\mathcal{D}}^2(\mathbf{L}, \mathbf{P}, \mathbf{Q}) + 4(|\mathbf{L}_{(l)}| |\mathbf{L}_{(q)}| \cos \theta)^2} \simeq \frac{\pi}{2 |\mathbf{L}_{(l)}| |\mathbf{L}_{(q)}|} \quad (\text{B14})$$

in the limit $\frac{\bar{\mathcal{D}}(\mathbf{L}, \mathbf{P}, \mathbf{Q})}{2 |\mathbf{L}_{(l)}| |\mathbf{L}_{(q)}|} \ll 1$, which is valid when $|\mathbf{L}_{(q)}|^2 \gg \frac{\Lambda}{(\lambda_{\text{cross}})^{\frac{1}{m+1}}}$. This follows from the fact that the main contribution to the integral over $|\mathbf{L}_{(l)}|$ comes from $|\mathbf{L}_{(l)}| \sim \tilde{\alpha}^{\frac{1}{3}} |\mathbf{L} - \mathbf{P}|^{\frac{d-m}{3}} \gg \Lambda$ in the large λ_{cross} limit. Using

$$\int d|\mathbf{L}_{(l)}| \frac{|\mathbf{L}_{(l)}|^{m-1}}{|\mathbf{L}_{(l)}|^3 + \tilde{\alpha} |\mathbf{L} - \mathbf{P}|^{d-m}} = \frac{\pi}{3 \sin\left(\frac{m\pi}{3}\right) |\mathbf{L} - \mathbf{P}|^{\frac{(d-m)(3-m)}{3}} \tilde{\alpha}^{\frac{(3-m)}{3}}} \quad \text{for } 0 < m < 3, \quad (\text{B15})$$

we perform the $|\mathbf{L}_{(l)}|$ -integral to obtain

$$\Pi_2(q) \sim -\frac{e^4 \mu^{2x} \pi}{48 N} \left(\frac{k_F}{12\pi}\right)^{\frac{m-1}{2}} \int \frac{d\mathbf{L} d\mathbf{P}}{(2\pi)^{2d-m}} \frac{\mathcal{B}_4(\mathbf{L}, \mathbf{P}, \mathbf{Q})}{\mathcal{D}_4(\mathbf{L}, \mathbf{P}, \mathbf{Q})} \frac{\pi}{|\mathbf{L}_{(q)}|^2 \tilde{\alpha}^{\frac{3-m}{3}} |\mathbf{L} - \mathbf{P}|^{\frac{(d-m)(3-m)}{3}} \sin\left(\frac{m\pi}{3}\right)}. \quad (\text{B16})$$

The total power of e comes out to be $\frac{2(m+3)}{3}$, and we find

$$\Pi_2(q) \sim -\frac{\tilde{e}^{\frac{m}{m+1}}}{k_F^{\frac{m-1}{2(m+1)}}} \frac{\left(e^2 k_F^{\frac{m-1}{2}}\right)^2 \pi^2}{48 N |\mathbf{L}_{(q)}|^2 \sin\left(\frac{m\pi}{3}\right)} \int \frac{d\mathbf{L} d\mathbf{P}}{(2\pi)^{2d-m}} \frac{\mathcal{B}_4(\mathbf{L}, \mathbf{P}, \mathbf{Q})}{\mathcal{D}_4(\mathbf{L}, \mathbf{P}, \mathbf{Q}) |\mathbf{L} - \mathbf{P}|^{\frac{(d-m)(3-m)}{3}}} \sim \frac{\tilde{e}^{\frac{m}{m+1}}}{k_F^{\frac{m-1}{2(m+1)}}} \frac{|\mathbf{Q}|^{\frac{m}{m+1}}}{N |\mathbf{L}_{(q)}|} \Pi_1(q), \quad (\text{B17})$$

to leading order in $|\mathbf{Q}|$ and ϵ . Therefore, the two-loop diagram is suppressed not only by a higher power of \tilde{e} but also by $\left(\frac{|\mathbf{Q}|}{k_F}\right)^{\frac{m-1}{2(m+1)}}$ compared to the one-loop diagram.

2. Two-loop contribution to fermion self-energy

The two-loop fermion self-energy in Fig. 8(a) is given by

$$\Sigma_2(q) = \frac{(ie)^4 \mu^{2x}}{N^2} \int dp dl D_1(p) D_1(l) \gamma_{d-m} G_0(p+q) \gamma_{d-m} G_0(p+l+q) \gamma_{d-m} G_0(l+q) \gamma_{d-m}. \quad (\text{B18})$$

Using the gamma matrix algebra, we find that the self-energy can be divided into two parts:

$$\Sigma_2(q) = \Sigma_{2a}(q) + \Sigma_{2b}(q), \quad (\text{B19})$$

where

$$\Sigma_{2a,2b}(q) = \frac{ie^4 \mu^{2x}}{N^2} \int dp dl D_1(p) D_1(l) \frac{\mathcal{C}_{a,b}}{[(\mathbf{P} + \mathbf{Q})^2 + \delta_{p+q}^2][(\mathbf{P} + \mathbf{L} + \mathbf{Q})^2 + \delta_{p+l+q}^2][(\mathbf{L} + \mathbf{Q})^2 + \delta_{l+q}^2]}, \quad (\text{B20})$$

with

$$\mathcal{C}_a = \gamma_{d-m} \left[\delta_{p+q} \delta_{p+l+q} \delta_{l+q} - \delta_{l+q} \{ \boldsymbol{\Gamma} \cdot (\mathbf{P} + \mathbf{Q}) \} \{ \boldsymbol{\Gamma} \cdot (\mathbf{P} + \mathbf{L} + \mathbf{Q}) \} - \delta_{p+q} \{ \boldsymbol{\Gamma} \cdot (\mathbf{P} + \mathbf{L} + \mathbf{Q}) \} \{ \boldsymbol{\Gamma} \cdot (\mathbf{L} + \mathbf{Q}) \} \right. \\ \left. - \delta_{p+l+q} \{ \boldsymbol{\Gamma} \cdot (\mathbf{P} + \mathbf{Q}) \} \{ \boldsymbol{\Gamma} \cdot (\mathbf{L} + \mathbf{Q}) \} \right], \quad (\text{B21})$$

$$\mathcal{C}_b = [\boldsymbol{\Gamma} \cdot (\mathbf{P} + \mathbf{Q})] [\boldsymbol{\Gamma} \cdot (\mathbf{P} + \mathbf{L} + \mathbf{Q})] [\boldsymbol{\Gamma} \cdot (\mathbf{L} + \mathbf{Q})] - \delta_{p+q} \delta_{l+q} [\boldsymbol{\Gamma} \cdot (\mathbf{P} + \mathbf{L} + \mathbf{Q})] - \delta_{p+l+q} \delta_{l+q} [\boldsymbol{\Gamma} \cdot (\mathbf{P} + \mathbf{Q})] \\ - \delta_{p+q} \delta_{p+l+q} [\boldsymbol{\Gamma} \cdot (\mathbf{L} + \mathbf{Q})]. \quad (\text{B22})$$

Shifting the variables as

$$p_{d-m} \rightarrow p_{d-m} - \delta_q - 2 \mathbf{L}_{(p)} \cdot \mathbf{L}_{(q)} - \mathbf{L}_{(p)}^2, \quad l_{d-m} \rightarrow l_{d-m} - \delta_q - 2 \mathbf{L}_{(l)} \cdot \mathbf{L}_{(q)} - \mathbf{L}_{(l)}^2,$$

and integrating over p_{d-m} and l_{d-m} , we obtain

$$\Sigma_{2a}(q) = \frac{i e^4 \mu^{2x}}{4 N^2} \int \frac{d\mathbf{P} d\mathbf{L}}{(2\pi)^{2d-2m}} \frac{d\mathbf{L}_{(p)} d\mathbf{L}_{(l)}}{(2\pi)^{2m}} \frac{\gamma_{d-m} (\delta_q - 2\mathbf{L}_{(l)} \cdot \mathbf{L}_{(p)}) \bar{C}_a(\mathbf{L}, \mathbf{P}, \mathbf{Q}) D_1(p) D_1(l)}{(\delta_q - 2\mathbf{L}_{(l)} \cdot \mathbf{L}_{(p)})^2 + \bar{C}(\mathbf{L}, \mathbf{P}, \mathbf{Q})^2}, \quad (\text{B23})$$

$$\Sigma_{2b}(q) = \frac{i e^4 \mu^{2x}}{4 N^2} \int \frac{d\mathbf{P} d\mathbf{L}}{(2\pi)^{2d-2m}} \frac{d\mathbf{L}_{(p)} d\mathbf{L}_{(l)}}{(2\pi)^{2m}} \frac{\bar{C}(\mathbf{L}, \mathbf{P}, \mathbf{Q}) \bar{C}_b(\mathbf{L}, \mathbf{P}, \mathbf{Q}) D_1(p) D_1(l)}{(\delta_q - 2\mathbf{L}_{(l)} \cdot \mathbf{L}_{(p)})^2 + \bar{C}(\mathbf{L}, \mathbf{P}, \mathbf{Q})^2}, \quad (\text{B24})$$

where

$$\begin{aligned} \bar{C}(\mathbf{L}, \mathbf{P}, \mathbf{Q}) &= |\mathbf{P} + \mathbf{Q}| + |\mathbf{L} + \mathbf{Q}| + |\mathbf{P} + \mathbf{L} + \mathbf{Q}|, \\ \bar{C}_a(\mathbf{L}, \mathbf{P}, \mathbf{Q}) &= 1 - \frac{[\mathbf{\Gamma} \cdot (\mathbf{P} + \mathbf{Q})][\mathbf{\Gamma} \cdot (\mathbf{P} + \mathbf{L} + \mathbf{Q})]}{|\mathbf{P} + \mathbf{Q}| |\mathbf{P} + \mathbf{L} + \mathbf{Q}|} - \frac{[\mathbf{\Gamma} \cdot (\mathbf{P} + \mathbf{L} + \mathbf{Q})][\mathbf{\Gamma} \cdot (\mathbf{L} + \mathbf{Q})]}{|\mathbf{P} + \mathbf{L} + \mathbf{Q}| |\mathbf{L} + \mathbf{Q}|} + \frac{[\mathbf{\Gamma} \cdot (\mathbf{P} + \mathbf{Q})][\mathbf{\Gamma} \cdot (\mathbf{L} + \mathbf{Q})]}{|\mathbf{P} + \mathbf{Q}| |\mathbf{L} + \mathbf{Q}|}, \\ \bar{C}_b(\mathbf{L}, \mathbf{P}, \mathbf{Q}) &= \frac{[\mathbf{\Gamma} \cdot (\mathbf{P} + \mathbf{Q})][\mathbf{\Gamma} \cdot (\mathbf{P} + \mathbf{L} + \mathbf{Q})][\mathbf{\Gamma} \cdot (\mathbf{L} + \mathbf{Q})]}{|\mathbf{P} + \mathbf{Q}| |\mathbf{P} + \mathbf{L} + \mathbf{Q}| |\mathbf{L} + \mathbf{Q}|} - \frac{[\mathbf{\Gamma} \cdot (\mathbf{L} + \mathbf{Q})]}{|\mathbf{L} + \mathbf{Q}|} + \frac{[\mathbf{\Gamma} \cdot (\mathbf{L} + \mathbf{P} + \mathbf{Q})]}{|\mathbf{L} + \mathbf{P} + \mathbf{Q}|} - \frac{[\mathbf{\Gamma} \cdot (\mathbf{P} + \mathbf{Q})]}{|\mathbf{P} + \mathbf{Q}|}. \end{aligned} \quad (\text{B25})$$

We can extract the UV divergent parts by expanding the integrand for small δ_q in Eq. (B23), and by setting $\delta_q = 0$ in Eq. (B24). In this limit, we have:

$$\Sigma_{2a}(q) = \frac{i e^4 \mu^{2x}}{4 N^2} \int \frac{d\mathbf{P} d\mathbf{L} d\mathbf{L}_{(p)} d\mathbf{L}_{(l)}}{(2\pi)^{2d}} \frac{\gamma_{d-m} \delta_q \bar{C}_a(\mathbf{L}, \mathbf{P}, \mathbf{Q}) D_1(p) D_1(l) \{\bar{C}(\mathbf{L}, \mathbf{P}, \mathbf{Q})^2 - 4(\mathbf{L}_{(l)} \cdot \mathbf{L}_{(p)})^2\}}{\{\bar{C}(\mathbf{L}, \mathbf{P}, \mathbf{Q})^2 + 4(\mathbf{L}_{(l)} \cdot \mathbf{L}_{(p)})^2\}^2}, \quad (\text{B26})$$

$$\Sigma_{2b}(q) = \frac{i e^4 \mu^{2x}}{4 N^2} \int \frac{d\mathbf{P} d\mathbf{L}}{(2\pi)^{2d-2m}} \frac{d\mathbf{L}_{(p)} d\mathbf{L}_{(l)}}{(2\pi)^{2m}} \frac{\bar{C}(\mathbf{L}, \mathbf{P}, \mathbf{Q}) \bar{C}_b(\mathbf{L}, \mathbf{P}, \mathbf{Q}) D_1(p) D_1(l)}{4(\mathbf{L}_{(l)} \cdot \mathbf{L}_{(p)})^2 + \bar{C}(\mathbf{L}, \mathbf{P}, \mathbf{Q})^2}. \quad (\text{B27})$$

For $m > 1$, the angular integrals along the Fermi surface directions give a factor proportional to

$$\int_0^\pi d\theta \frac{\bar{C}^2(\mathbf{L}, \mathbf{P}, \mathbf{Q}) - 4(|\mathbf{L}_{(l)}| |\mathbf{L}_{(p)}| \cos \theta)^2}{\{\bar{C}(\mathbf{L}, \mathbf{P}, \mathbf{Q})^2 + 4(|\mathbf{L}_{(l)}| |\mathbf{L}_{(p)}| \cos \theta)^2\}^2} \sin^{m-2} \theta \simeq \begin{cases} \frac{\sqrt{\pi} \Gamma(\frac{m-1}{2})}{\bar{C}^2 \Gamma(\frac{m}{2})}, & \text{for } \frac{\bar{C}(\mathbf{L}, \mathbf{P}, \mathbf{Q})}{2|\mathbf{L}_{(l)}| |\mathbf{L}_{(p)}|} \gg 1, \\ \frac{\sqrt{\pi} \Gamma(\frac{m-1}{2})}{2\mathbf{L}_{(l)}^2 \mathbf{L}_{(p)}^2 \Gamma(\frac{m}{2}-1)} + \frac{\pi(3-m)\bar{C}}{8|\mathbf{L}_{(l)}|^3 |\mathbf{L}_{(p)}|^3}, & \text{for } \frac{\bar{C}(\mathbf{L}, \mathbf{P}, \mathbf{Q})}{2|\mathbf{L}_{(l)}| |\mathbf{L}_{(p)}|} \ll 1, \end{cases} \quad (\text{B28})$$

for Σ_{2a} ; and

$$\int_0^\pi d\theta \frac{\bar{C}(\mathbf{L}, \mathbf{P}, \mathbf{Q}) \sin^{m-2} \theta}{\bar{C}^2(\mathbf{L}, \mathbf{P}, \mathbf{Q}) + 4(|\mathbf{L}_{(l)}| |\mathbf{L}_{(p)}| \cos \theta)^2} \simeq \begin{cases} \frac{\sqrt{\pi} \Gamma(\frac{m-1}{2})}{\bar{C} \Gamma(\frac{m}{2})}, & \text{for } \frac{\bar{C}(\mathbf{L}, \mathbf{P}, \mathbf{Q})}{2|\mathbf{L}_{(l)}| |\mathbf{L}_{(p)}|} \gg 1, \\ \frac{\pi}{2|\mathbf{L}_{(l)}| |\mathbf{L}_{(p)}|} - \frac{\sqrt{\pi} \bar{C} \Gamma(\frac{m-1}{2})}{2\mathbf{L}_{(l)}^2 \mathbf{L}_{(p)}^2 \Gamma(\frac{m}{2}-1)}, & \text{for } \frac{\bar{C}(\mathbf{L}, \mathbf{P}, \mathbf{Q})}{2|\mathbf{L}_{(l)}| |\mathbf{L}_{(p)}|} \ll 1, \end{cases} \quad (\text{B29})$$

for Σ_{2b} . For $\frac{\bar{C}(\mathbf{L}, \mathbf{P}, \mathbf{Q})}{2|\mathbf{L}_{(l)}| |\mathbf{L}_{(p)}|} \ll 1$, the leading and the second leading order terms in $\frac{\bar{C}(\mathbf{L}, \mathbf{P}, \mathbf{Q})}{2|\mathbf{L}_{(l)}| |\mathbf{L}_{(p)}|}$ are kept. Although the second leading term is not important for Σ_{2b} , it plays an important role for Σ_{2a} at $m = 2$ because the leading term vanishes at $m = 2$.

Let us first estimate Σ_{2a} . It is convenient to perform the integrations for $\mathbf{L}_{(l)}$ and $\mathbf{L}_{(p)}$ in the four regions separately,

$$\begin{aligned} &\left\{ 0 < |\mathbf{L}_{(l)}| < \frac{\bar{C}}{2|\mathbf{L}_{(p)}|}, \quad 0 < |\mathbf{L}_{(p)}| < \frac{\bar{C}}{2\tilde{\alpha}^{\frac{1}{3}} |\mathbf{L}|^{\frac{d-m}{3}}} \right\}, \\ &\left\{ 0 < |\mathbf{L}_{(l)}| < \frac{\bar{C}}{2|\mathbf{L}_{(p)}|}, \quad \frac{\bar{C}}{2\tilde{\alpha}^{\frac{1}{3}} |\mathbf{L}|^{\frac{d-m}{3}}} < |\mathbf{L}_{(p)}| < \infty \right\}, \\ &\left\{ \frac{\bar{C}}{2|\mathbf{L}_{(p)}|} < |\mathbf{L}_{(l)}| < \infty, \quad 0 < |\mathbf{L}_{(p)}| < \frac{\bar{C}}{2\tilde{\alpha}^{\frac{1}{3}} |\mathbf{L}|^{\frac{d-m}{3}}} \right\}, \\ &\left\{ \frac{\bar{C}}{2|\mathbf{L}_{(p)}|} < |\mathbf{L}_{(l)}| < \infty, \quad \frac{\bar{C}}{2\tilde{\alpha}^{\frac{1}{3}} |\mathbf{L}|^{\frac{d-m}{3}}} < |\mathbf{L}_{(p)}| < \infty \right\}. \end{aligned} \quad (\text{B30})$$

Adding the result of integrations in each region, we obtain

$$\begin{aligned} \Sigma_{2a}(q) \sim \frac{i e^4 \mu^{2x} \gamma_{d-m} \delta_q \pi}{4 N^2} \int \frac{d\mathbf{P} d\mathbf{L}}{(2\pi)^{2d}} \bar{\mathcal{C}}_a(\mathbf{L}, \mathbf{P}, 0) \left[\frac{\pi^{\frac{3}{2}} \Gamma\left(\frac{m-1}{2}\right) \sec^2\left(\frac{(2m+1)\pi}{3}\right)}{18 \Gamma\left(\frac{m}{2} - 1\right) \tilde{\alpha}^{\frac{2(4-m)}{3}} (|\mathbf{L}| |\mathbf{P}|)^{\frac{(d-m)(4-m)}{3}}} \right. \\ \left. + \frac{\bar{\mathcal{C}}^{m-1}(\mathbf{L}, \mathbf{P}, 0)}{8 \tilde{\alpha}^2 (|\mathbf{L}| |\mathbf{P}|)^{d-m}} \left\{ \frac{2^{2-m} (m+4-3(m+1) \log \mathcal{A}) \Gamma\left(\frac{m-1}{2}\right)}{3 \sqrt{\pi} (m+1)^2 \Gamma\left(\frac{m}{2}\right)} + \frac{\frac{\mathcal{A}^{2-m}-1}{2-m} - \log \mathcal{A}}{2^{m-2}(2-m)/(3-m)} \right. \right. \\ \left. \left. + \frac{2^{2-m} (3-m)}{3} \frac{1 - \frac{3\mathcal{A}^{2-m}}{5-m}}{2-m} + \frac{3-m}{5-m} \frac{2^{2-m} (1 - \mathcal{A}^{2-m})}{2-m} + \frac{2^{2-m} (3-m) (1 + 3\mathcal{A}^{2-m})}{3(5-m)^2} \right\} \right], \end{aligned} \quad (\text{B31})$$

where

$$\mathcal{A}(\mathbf{L}, \mathbf{P}, \alpha) = \frac{\bar{\mathcal{C}}(\mathbf{L}, \mathbf{P}, 0)}{2 (|\mathbf{L}| |\mathbf{P}|)^{\frac{d-m}{3}} \tilde{\alpha}^{\frac{2}{3}}}. \quad (\text{B32})$$

Here \mathbf{Q} dependent terms are dropped because they are sub-leading compared to the one that depends on δ_q . Note that $\frac{\mathcal{A}^{2-m}-1}{2-m}$ and $\frac{\frac{\mathcal{A}^{2-m}-1}{2-m} - \log \mathcal{A}}{2^{m-2}(2-m)/(3-m)}$ become terms that include $\log \mathcal{A}$ and $\log^2 \mathcal{A}$ at $m = 2$. From similar integrations, $\Sigma_{2b}(q)$ is evaluated to be

$$\Sigma_{2b}(q) \sim \frac{i e^4 \mu^{2x} \pi^3}{72 N^2} \int \frac{d\mathbf{P} d\mathbf{L}}{(2\pi)^{2d}} \frac{\bar{\mathcal{C}}_b(\mathbf{L}, \mathbf{P}, \mathbf{Q})}{\tilde{\alpha}^{\frac{2(3-m)}{3}} (|\mathbf{L}| |\mathbf{P}|)^{\frac{(d-m)(3-m)}{3}} \sin^2\left(\frac{m\pi}{3}\right)}. \quad (\text{B33})$$

For $d = d_c - \epsilon$, we find that

$$\begin{aligned} \Sigma_{2a}(q) \sim \frac{i \gamma_{d-m} \delta_q \pi}{4 N^2} \int \frac{d\mathbf{P} d\mathbf{L}}{(2\pi)^{2d}} \bar{\mathcal{C}}_a(\mathbf{L}, \mathbf{P}, 0) \left[\frac{\tilde{e}^{\frac{2(m-1)}{m+1}} \pi^{\frac{3}{2}} \Gamma\left(\frac{m-1}{2}\right) \sec^2\left(\frac{(2m+1)\pi}{3}\right)}{k_F^{\frac{2(m-1)}{m+1}} 18 \Gamma\left(\frac{m}{2} - 1\right) (|\mathbf{L}| |\mathbf{P}|)^{\frac{(d-m)(4-m)}{3}}} \right. \\ \left. + \frac{\bar{\mathcal{C}}^{m-1}(\mathbf{L}, \mathbf{P}, 0)}{8 k_F^{m-1} (|\mathbf{L}| |\mathbf{P}|)^{d-m}} \left\{ \frac{2^{2-m} (m+4-3(m+1) \log \mathcal{A}) \Gamma\left(\frac{m-1}{2}\right)}{3 \sqrt{\pi} (m+1)^2 \Gamma\left(\frac{m}{2}\right)} + \frac{\left(\frac{\mathcal{A}|\tilde{\alpha}=1}{\tilde{e}^{\frac{2}{m+1}} k_F^{\frac{m-1}{m+1}} \beta_d^{\frac{2}{3}}}\right)^{2-m} - 1}{2^{m-2}(2-m)/(3-m)} - \log \mathcal{A} \right. \right. \\ \left. \left. + \frac{2^{2-m} (3-m)}{3} \frac{1 - \frac{3}{5-m} \left(\frac{\mathcal{A}|\tilde{\alpha}=1}{\tilde{e}^{\frac{2}{m+1}} k_F^{\frac{m-1}{m+1}} \beta_d^{\frac{2}{3}}}\right)^{2-m}}{2-m} + \frac{3-m}{5-m} \frac{1 - \left(\frac{\mathcal{A}|\tilde{\alpha}=1}{\tilde{e}^{\frac{2}{m+1}} k_F^{\frac{m-1}{m+1}} \beta_d^{\frac{2}{3}}}\right)^{2-m}}{2^{m-2}(2-m)} + \frac{1 + 3 \left(\frac{\mathcal{A}|\tilde{\alpha}=1}{\tilde{e}^{\frac{2}{m+1}} k_F^{\frac{m-1}{m+1}} \beta_d^{\frac{2}{3}}}\right)^{2-m}}{2^{m-2} \times 3(5-m)^2/(3-m)} \right\} \right], \end{aligned} \quad (\text{B34})$$

and

$$\Sigma_{2b}(q) \sim \frac{\tilde{e}^{\frac{2m}{m+1}}}{k_F^{\frac{m-1}{m+1}}} \frac{i \pi^3}{72 N^2} \int \frac{d\mathbf{P} d\mathbf{L}}{(2\pi)^{2d}} \frac{\bar{\mathcal{C}}_b(\mathbf{L}, \mathbf{P}, \mathbf{Q})}{(|\mathbf{L}| |\mathbf{P}|)^{\frac{(d-m)(3-m)}{3}} \sin^2\left(\frac{m\pi}{3}\right)} \sim \tilde{e}^{\frac{2m}{m+1}} \left(\frac{\Lambda}{k_F}\right)^{\frac{m-1}{m+1}} \frac{i \mathbf{\Gamma} \cdot \mathbf{Q}}{N^2} \quad (\text{B35})$$

to leading order in δ_q , \mathbf{Q} and ϵ . The two-loop fermion self-energy is suppressed by \tilde{e} and $\frac{\Lambda}{k_F}$ at low energies for $m > 1$. Due to the Ward identity, the two-loop vertex corrections shown in Fig. 9 are also suppressed. It is noted that Eqs. (B34) and (B35) are finite in the $\epsilon \rightarrow 0$ limit. This is because the Fermi energy k_F enters as a dimensional parameter that further suppresses the two-loop contributions compared to the one-loop diagrams. Therefore the critical exponents do not receive quantum corrections from the two-loop diagrams in the low-energy limit.